

# The Dynamic Two-Fluid Model OLGA: Theory and Application

Kjell H. Bendiksen, Dag Malnes, Randi Moe, and Sven Nuland, Inst. for Energy Technology

SPE 19451

**Summary.** Dynamic two-fluid models have found a wide range of application in the simulation of two-phase-flow systems, particularly for the analysis of steam/water flow in the core of a nuclear reactor. Until quite recently, however, very few attempts have been made to use such models in the simulation of two-phase oil and gas flow in pipelines. This paper presents a dynamic two-fluid model, OLGA, in detail, stressing the basic equations and the two-fluid models applied. Predictions of steady-state pressure drop, liquid holdup, and flow-regime transitions are compared with data from the SINTEF Two-Phase Flow Laboratory and from the literature. Comparisons with evaluated field data are also presented.

## Introduction

The development of the dynamic two-phase-flow model OLGA started as a project for Statoil to simulate slow transients associated with mass transport, rather than the fast pressure transients well known from the nuclear industry. Problems of interest included terrain slugging, pipeline startup and shut-in, variable production rates, and pigging. This implied simulations with time spans ranging from hours to weeks in extreme cases. Thus, the numerical method applied would have to be stable for long timesteps and not restricted by the velocity of sound.

A first version of OLGA based on this approach was working in 1983, but the main development was carried out in a joint research program between the Inst. for Energy Technology (IFE) and SINTEF, supported by Conoco Norway, Esso Norge, Mobil Exploration Norway, Norsk Hydro A/S, Petro Canada, Saga Petroleum, Statoil, and Texaco Exploration Norway. In this project, the empirical basis of the model was extended and new applications were introduced. To a large extent, the present model is a product of this project.

Two-phase flow traditionally has been modeled by separate empirical correlations for volumetric gas fraction, pressure drop, and flow regimes, although these are physically interrelated. In recent years, however, advanced dynamic nuclear reactor codes like TRAC,<sup>11</sup> RELAP-5,<sup>2</sup> and CATHARE<sup>3</sup> have been developed and are based on a more unified approach to gas fraction and pressure drop. Flow regimes, however, are still treated by separate flow-regime maps as functions of void fraction and mass flow only. In the OLGA approach, flow regimes are treated as an integral part of the two-fluid system.

The physical model of OLGA was originally based on small-diameter data for low-pressure air/water flow. The 1983 data from the SINTEF Two-Phase Flow Laboratory showed that, while the bubble/sluggish flow regime was described adequately, the stratified/annular regime was not. In vertical annular flow, the predicted pressure drops were up to 50% too high (see Fig. 1). In horizontal flow, the predicted holdups were too high by a factor of two in extreme cases.

These discrepancies were explained by the neglect of a droplet field, moving at approximately the gas velocity, in the early model. This regime, denoted stratified- or annular-mist flow, has been incorporated in OLGA 84 and later versions, where the liquid flow may be in the form of a wall layer and a possible droplet flow in the gas core.

This paper describes the basic features of this extended two-fluid model, emphasizing its differences with other known two-fluid models.

## OLGA—The Extended Two-Fluid Model

**Physical Models.** Separate continuity equations are applied for gas, liquid bulk, and liquid droplets, which may be coupled through interphasial mass transfer. Only two momentum equations are used, however: a combined equation for the gas and possible liquid droplets and a separate one for the liquid film. A mixture energy-conservation equation currently is applied.

**Conservation of Mass.** For the gas phase,

$$\frac{\partial}{\partial t}(V_g \rho_g) = -\frac{1}{A} \frac{\partial}{\partial z}(AV_g \rho_g v_g) + \psi_g + G_g. \quad (1)$$

For the liquid phase at the wall,

$$\frac{\partial}{\partial t}(V_L \rho_L) = -\frac{1}{A} \frac{\partial}{\partial z}(AV_L \rho_L v_L) - \psi_g \frac{V_L}{V_L + V_D} - \psi_e + \psi_d + G_L. \quad (2)$$

For liquid droplets,

$$\frac{\partial}{\partial t}(V_D \rho_L) = -\frac{1}{A} \frac{\partial}{\partial z}(AV_D \rho_L v_D) - \psi_g \frac{V_D}{V_L + V_D} + \psi_e - \psi_d + G_D. \quad (3)$$

In Eqs. 1 through 3,  $V_g, V_L, V_D$  = gas, liquid-film, and liquid-droplet volume fractions,  $\rho$  = density,  $v$  = velocity,  $p$  = pressure, and  $A$  = pipe cross-sectional area.  $\psi_g$  = mass-transfer rate between the phases,  $\psi_e$ ,  $\psi_d$  = the entrainment and deposition rates, and  $G_f$  = possible mass source of Phase f. Subscripts g, L, i, and D indicate gas, liquid, interface, and droplets, respectively.

**Conservation of Momentum.** Conservation of momentum is expressed for three different fields, yielding the following separate 1D momentum equations for the gas, possible liquid droplets, and liquid bulk or film.

For the gas phase,

$$\begin{aligned} \frac{\partial}{\partial t}(V_g \rho_g v_g) &= -V_g \left( \frac{\partial p}{\partial z} \right) - \frac{1}{A} \frac{\partial}{\partial z}(AV_g \rho_g v_g^2) - \lambda_g \frac{1}{2} \rho_g |v_g| v_g \\ &\times \frac{S_g}{4A} - \lambda_i \frac{1}{2} \rho_g |v_r| v_r \frac{S_i}{4A} + V_g \rho_g g \cos \alpha + \psi_g v_a - F_D. \end{aligned} \quad (4)$$

For liquid droplets,

$$\begin{aligned} \frac{\partial}{\partial t}(V_D \rho_L v_D) &= -V_D \left( \frac{\partial p}{\partial z} \right) - \frac{1}{A} \frac{\partial}{\partial z}(AV_D \rho_L v_D^2) + V_D \rho_L g \cos \alpha \\ &- \psi_g \frac{V_D}{V_L + V_D} v_a + \psi_e v_i - \psi_d v_D + F_D. \end{aligned} \quad (5)$$

Eqs. 4 and 5 were combined to yield a combined momentum equation, where the gas/droplet drag terms,  $F_D$ , cancel out:

$$\begin{aligned} \frac{\partial}{\partial t}(V_g \rho_g v_g + V_D \rho_L v_D) &= -(V_g + V_D) \left( \frac{\partial p}{\partial z} \right) - \frac{1}{A} \frac{\partial}{\partial z}(AV_g \rho_g v_g^2) \\ &+ AV_D \rho_L v_D^2 - \lambda_g \frac{1}{2} \rho_g |v_g| v_g \frac{S_g}{4A} - \lambda_i \frac{1}{2} \rho_g |v_r| v_r \frac{S_i}{4A} \\ &+ (V_g \rho_g + V_D \rho_L) g \cos \alpha + \psi_g \frac{V_L}{V_L + V_D} v_a + \psi_e v_i - \psi_d v_D. \end{aligned} \quad (6)$$

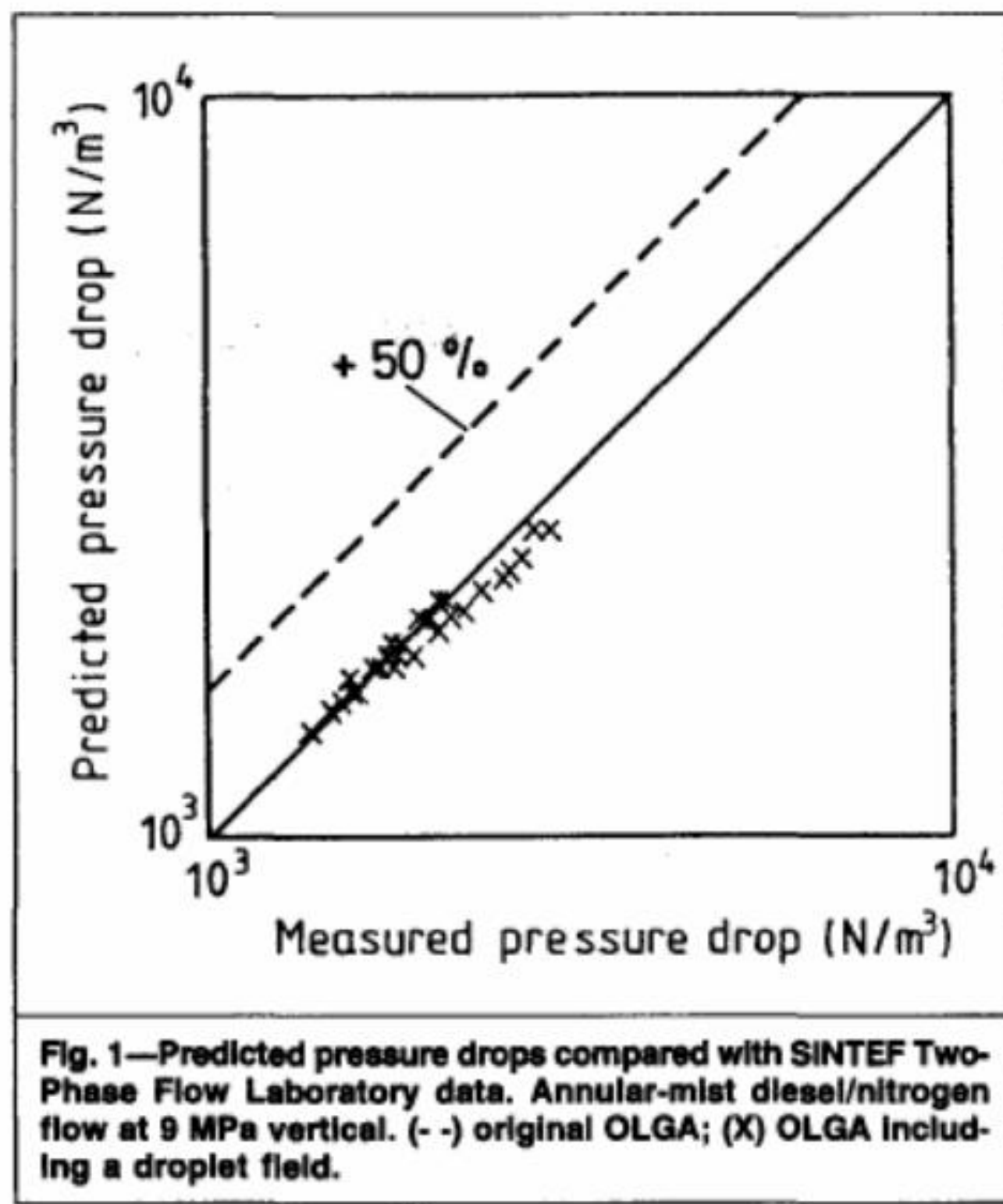


**Fig. 1—Predicted pressure drops compared with SINTEF Two-Phase Flow Laboratory data. Annular-mist diesel/nitrogen flow at 9 MPa vertical. (--) original OLGA; (X) OLGA Including a droplet field.**

For the liquid at the wall,

$$\begin{aligned} \frac{\partial}{\partial t}(V_L \rho_L v_L) &= -V_L \left( \frac{\partial p}{\partial z} \right) - \frac{1}{A} \frac{\partial}{\partial z}(AV_L \rho_L v_L^2) \\ -\lambda_L \frac{1}{2} \rho_L |v_L| v_L \frac{S_L}{4A} + \lambda_i \frac{1}{2} \rho_g |v_r| v_r \frac{S_i}{4A} &+ V_L \rho_L g \cos \alpha \\ -\psi_g \frac{V_L}{V_L + V_D} v_a - \psi_e v_i + \psi_d v_D - V_L d(\rho_L - \rho_g) g \frac{\partial V_L}{\partial z} \sin \alpha. & \end{aligned} \quad (7)$$

In Eqs. 4 through 7,  $\alpha$ =pipe inclination with the vertical and  $S_g$ ,  $S_L$ , and  $S_i$ =wetted perimeters of the gas, liquid, and interface. The internal source,  $G_f$ , is assumed to enter at a  $90^\circ$  angle to the pipe wall, carrying no net momentum.

$$v_a = v_L \text{ for } \psi_g > 0 \quad (8a)$$

(and evaporation from the liquid film),

$$v_a = v_D \text{ for } \psi_g < 0 \quad (8b)$$

(and evaporation from the liquid droplets),

$$\text{and } v_a = v_g \text{ for } \psi_g < 0 \quad (8c)$$

(condensation).

The above conservation equations can be applied for all flow regimes. Observe, however, that certain terms may drop out for certain flow regimes; e.g., in slug or dispersed bubble flow, all the droplet terms disappear.

For slug flow, the frictional pressure-drop terms are composite. They consist of three terms, owing to the liquid slug, the slug bubble and the film under it, and the liquid-film-acceleration pressure drop.

The relative velocity,  $v_r$ , is defined by the following slip equation:

$$v_g = R_D(v_L + v_r), \quad (9)$$

where  $R_D$  is a distribution slip ratio caused by an uneven distribution of phases and velocities across the pipe cross section, as outlined in the next section.

The droplet velocity is similarly defined by

$$v_D = v_g - v_{0D} \cos \alpha, \dots \quad (10)$$

where  $v_{0D}$  is the fall velocity of droplets. The interphase velocity,  $v_i$ , is approximated by  $v_L$ .

**Pressure Equation.** OLGA reformulates the problem before discretizing the differential equations to obtain a pressure equation. This equation, together with the momentum equations, may be solved simultaneously for the pressure and phase velocities and thus allow a stepwise time integration.

The conservation-of-mass equations (Eqs. 1 through 3) may be expanded with respect to pressure, temperature, and composition, assuming that the densities are given as

$$\rho_f = \rho_f(p, T, R_s), \dots \quad (11)$$

where the gas mass fraction,  $R_s$ , is defined by Eq. 17.

For the gas equation (Eq. 1), the left side may be expressed as

$$\begin{aligned} \frac{\partial V_g \rho_g}{\partial t} &= \rho_g \frac{\partial V_g}{\partial t} + V_g \frac{\partial \rho_g}{\partial t} = \rho_g \frac{\partial V_g}{\partial t} + V_g \left[ \left( \frac{\partial \rho_g}{\partial p} \right)_{T, R_s} \frac{\partial p}{\partial t} \right. \\ &\left. + \left( \frac{\partial \rho_g}{\partial T} \right)_{p, R_s} \frac{\partial T}{\partial t} + \left( \frac{\partial \rho_g}{\partial R_s} \right)_{p, T} \frac{\partial R_s}{\partial t} \right]. \end{aligned} \quad (12)$$

Dividing the expansions (Eq. 12) for each phase by the densities and adding the three equations yields a volume-conservation equation (neglecting the last two terms in Eq. 12 because they normally are negligible in pipeline transport problems owing to the slow temperature development):

$$\begin{aligned} \left[ \frac{V_g \left( \frac{\partial \rho_g}{\partial p} \right)_{T, R_s}}{\rho_g} + \frac{1 - V_g \left( \frac{\partial \rho_L}{\partial p} \right)_{T, R_s}}{\rho_L} \right] \frac{\partial p}{\partial t} &= \frac{1}{\rho_g} \frac{\partial m_g}{\partial t} \\ + \frac{1}{\rho_L} \frac{\partial m_L}{\partial t} + \frac{1}{\rho_D} \frac{\partial m_D}{\partial t}. & \end{aligned} \quad (13)$$

Inserting the mass-conservation equations for each phase and applying  $V_g + V_L + V_D = 1$  gives

$$\begin{aligned} \left[ \frac{V_g \left( \frac{\partial \rho_g}{\partial p} \right)_{T, R_s}}{\rho_g} + \frac{1 - V_g \left( \frac{\partial \rho_L}{\partial p} \right)_{T, R_s}}{\rho_L} \right] \frac{\partial p}{\partial t} &= -\frac{1}{A \rho_g} \frac{\partial (AV_g \rho_g v_g)}{\partial z} \\ -\frac{1}{A \rho_L} \frac{\partial (AV_L \rho_L v_L)}{\partial z} - \frac{1}{A \rho_D} \frac{\partial (AV_D \rho_D v_D)}{\partial z} + \psi_g \left( \frac{1}{\rho_g} - \frac{1}{\rho_L} \right) & \\ + G_g \frac{1}{\rho_g} + G_L \frac{1}{\rho_L} + G_D \frac{1}{\rho_D}. & \end{aligned} \quad (14)$$

Eq. 14 provides a single equation for the pressure and phase fluxes. Note that if the phase transfer term,  $\psi_g$ , is a function of pressure, temperature, and composition,

$$\psi_g = \psi_g(p, T, R_s), \quad (15)$$

then  $\psi_g$  may be expanded by a Taylor series in  $p$ ,  $T$ , and  $R_s$ , as shown in Eq. 18. A strong effect of pressure on the phase transfer (boiling) may then be incorporated into Eq. 14.

**Energy Equation.** A mixture energy-conservation equation is applied:

$$\begin{aligned} \frac{\partial}{\partial t} \left[ m_g \left( E_g + \frac{1}{2} v_g^2 + gh \right) + m_L \left( E_L + \frac{1}{2} v_L^2 + gh \right) \right. \\ \left. + m_D \left( E_D + \frac{1}{2} v_D^2 + gh \right) \right] &= -\frac{\partial}{\partial z} \left[ m_g v_g \left( H_g + \frac{1}{2} v_g^2 + gh \right) \right. \\ \left. + m_L v_L \left( H_L + \frac{1}{2} v_L^2 + gh \right) + m_D v_D \left( H_D + \frac{1}{2} v_D^2 + gh \right) \right] + H_S + U, \end{aligned} \quad (16)$$

where  $E$  = internal energy per unit mass,  $h$  = elevation,  $H_S$  = enthalpy from mass sources, and  $U$  = heat transfer from pipe walls.

**Thermal Calculations.** OLGA can simulate a pipeline with a totally insulated wall or with a wall composed of layers of different thicknesses, heat capacities, and conductivities. The wall description may change along the pipeline to simulate, for instance, a well surrounded by rock of a certain vertical temperature profile, connected to a flowline with insulating materials and concrete coating, and an uninsulated riser.

OLGA computes the heat-transfer coefficient from the flowing fluid to the internal pipe wall; the user specifies the heat-transfer coefficient on the outside. Circumferential symmetry is assumed; if this is broken, for example, with a partly buried pipe on the sea bottom, average heat-transfer coefficients must be specified.

Special phenomena, such as the Joule-Thompson effect, are included, provided that the PVT package applied to generate the fluid-property tables can describe such effects.

**Fluid Properties and Phase Transfer.** All fluid properties (densities, compressibilities, viscosities, surface tension, enthalpies, heat capacities, and thermal conductivities) are given as tables in pressure and temperature, and the actual values at a given point in time and space are found by interpolating in these tables.

The tables are generated before OLGA is run by use of any fluid-properties package, based on a Peng-Robinson, Soave-Redlich-Kwong, or another equation of state, complying with the specified table format.

The total mixture composition is assumed to be constant in time along the pipeline, while the gas and liquid compositions change with pressure and temperature as a result of interfacial mass transfer. In real systems, the velocity difference between the oil and gas phases may cause changes in the total composition of the mixture. This can be fully accounted for only in a compositional model.

**Interfacial Mass Transfer.** The applied interface mass-transfer model can treat both normal condensation or evaporation and retrograde condensation, in which a heavy phase condenses from the gas phase as the pressure drops. Defining a gas mass fraction at equilibrium conditions as

$$R_s = m_g / (m_g + m_L + m_D), \quad \dots \dots \dots (17)$$

we may compute the mass-transfer rate as

$$\begin{aligned} \psi_g = & \left[ \left( \frac{\partial R_s}{\partial p} \right)_T \frac{\partial p}{\partial t} + \left( \frac{\partial R_s}{\partial p} \right)_T \frac{\partial p}{\partial z} \frac{\partial z}{\partial t} \right. \\ & \left. + \left( \frac{\partial R_s}{\partial T} \right)_p \frac{\partial T}{\partial t} + \left( \frac{\partial R_s}{\partial T} \right)_p \frac{\partial T}{\partial z} \frac{\partial z}{\partial t} \right] (m_g + m_L + m_D). \quad \dots \dots \dots (18) \end{aligned}$$

The term  $(\partial R_s / \partial p)_T (\partial p / \partial t)$  represents the phase transfer from a mass present in a section owing to pressure change in that section. The term  $(\partial R_s / \partial p)_T (\partial p / \partial z) (\partial z / \partial t)$  represents the mass transfer caused by mass flowing from one section to the next. Because only derivatives of  $R_s$  appear in Eq. 18, errors resulting from the assumption of constant composition are minimized.

**Numerical Solution Scheme.** The physical problem, as formulated previously, yields a set of coupled first-order, nonlinear, 1D partial differential equations with rather complex coefficients. This nonlinearity means that no single numerical method is optimal from all points of view. In fact, the codes TRAC,<sup>1</sup> RELAP,<sup>2</sup> CATHARE,<sup>3</sup> and OLGA all use different solution schemes. Details are presented elsewhere.<sup>4</sup>

Most two-fluid models, including those listed above, apply finite-difference staggered mesh, donor cell methods. In explicit integration methods, the timestep,  $\Delta t$ , is limited by the Courant Friedrich Levy criterion based on the speed of sound:

$$\Delta t \leq \min \{ \Delta z_j / |v_{fj}| \pm c_{fj} | \}. \quad \dots \dots \dots (19)$$

Implicit methods are not limited by Eq. 19, but for dynamic problems a mass-transport criterion applies:

$$\Delta t \leq \min \{ \Delta z_j / |v_{fj}| \}. \quad \dots \dots \dots (20)$$

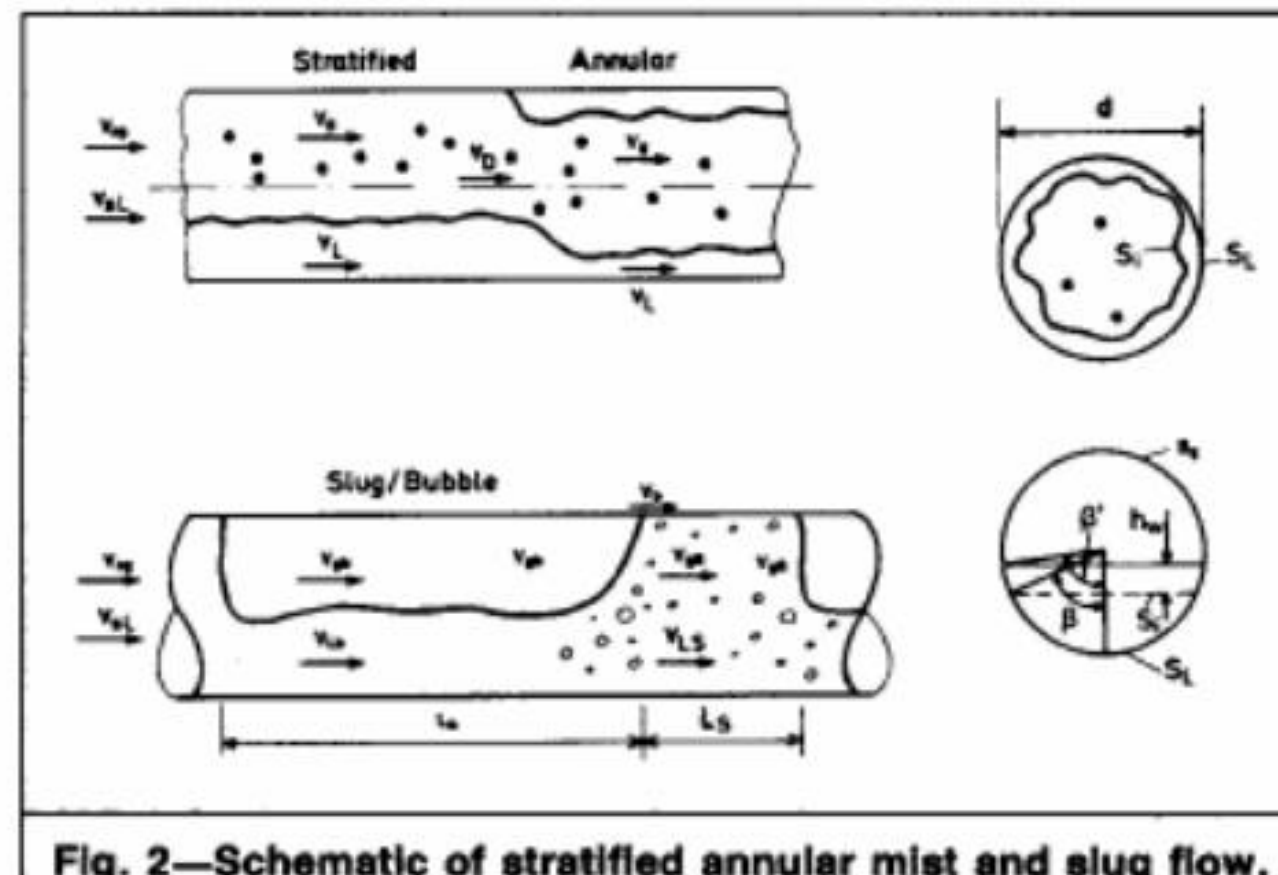


Fig. 2—Schematic of stratified annular mist and slug flow.

Because the speed of sound typically is about  $10^2$  to  $10^3$  times larger than the average phase velocities, explicit integration methods require timesteps up to  $10^3$  times smaller than implicit methods.

Traditionally, most nuclear reactor safety analysis codes (e.g., NORA<sup>5</sup>) applied explicit methods because they are simpler to formulate and code, and the time scales of interest for typical problems (pressure transients) were given by the speed of sound. Because of stability problems, however, and the need to simulate slow, small breaks, implicit methods are now favored.

### Flow-Regime Description

The friction factors and wetted perimeters depend on flow regime. Two basic flow-regime classes are applied: distributed, which contains bubble and slug flow, and separated, which contains stratified- and annular-mist flow. Because OLGA is a unified model, it does not require separate user-specified correlations for liquid holdup, etc. Thus, for each pipeline section, a dynamic flow-regime prediction is required, yielding the correct flow regime as a function of average flow parameters.

**Separated Flow.** Stratified- and annular-mist flows are characterized by the two phases moving separately (Fig. 2). The phase distributions across the respective phase areas are assumed constant. The distribution slip ratio,  $R_D$ , in Eq. 9 then becomes 1.0. The transition between stratified and annular flow is based on the wetted perimeter of the liquid film; annular flow results when this perimeter becomes equal to the film inner circumference.

Stratified flow may be either smooth or wavy. An expression for the average wave height,  $h_w$ , may be obtained by assuming that the mass flow forces in the gas balance the gravitational and surface tension forces, or

$$(1/2)\rho_g(v_g - v_L)^2 = h_w(\rho_L - \rho_g)g \sin \alpha + (\sigma/h_w) \quad \dots \dots \dots (21)$$

$$\text{or } h_w = \frac{1}{2} \left\{ \frac{\rho_g(v_g - v_L)^2}{2(\rho_L - \rho_g)g \sin \alpha} + \sqrt{\left[ \frac{\rho_g(v_g - v_L)^2}{2(\rho_L - \rho_g)g \sin \alpha} \right]^2 - \frac{4\sigma}{(\rho_L - \rho_g)g \sin \alpha}} \right\}. \quad \dots \dots \dots (22)$$

When the expression in the square root is negative,  $h_w$  is zero and stratified smooth flow is obtained.

The onset of waves starts with capillary waves with wavelengths of about 2 to 3 mm. As the mass-flow forces increase, surface tension becomes negligible and gravity dominates, resulting in longer wavelengths. For air/water pipe flow at 1 bar, the onset of 2D waves corresponds very well with the data of Andreussi and Persen<sup>6</sup> (Fig. 3).

**Friction Factors.** The applied wall friction factors for gas and liquid are those of either turbulent or laminar flow (in practice, the maximum one is chosen), given as

$$\lambda_f = 0.0055 \left[ 1 + \left( \frac{2 \times 10^4 \epsilon}{d_h} + \frac{10^6}{N_{Re}} \right)^{1/4} \right] \quad \dots \dots \dots (23)$$

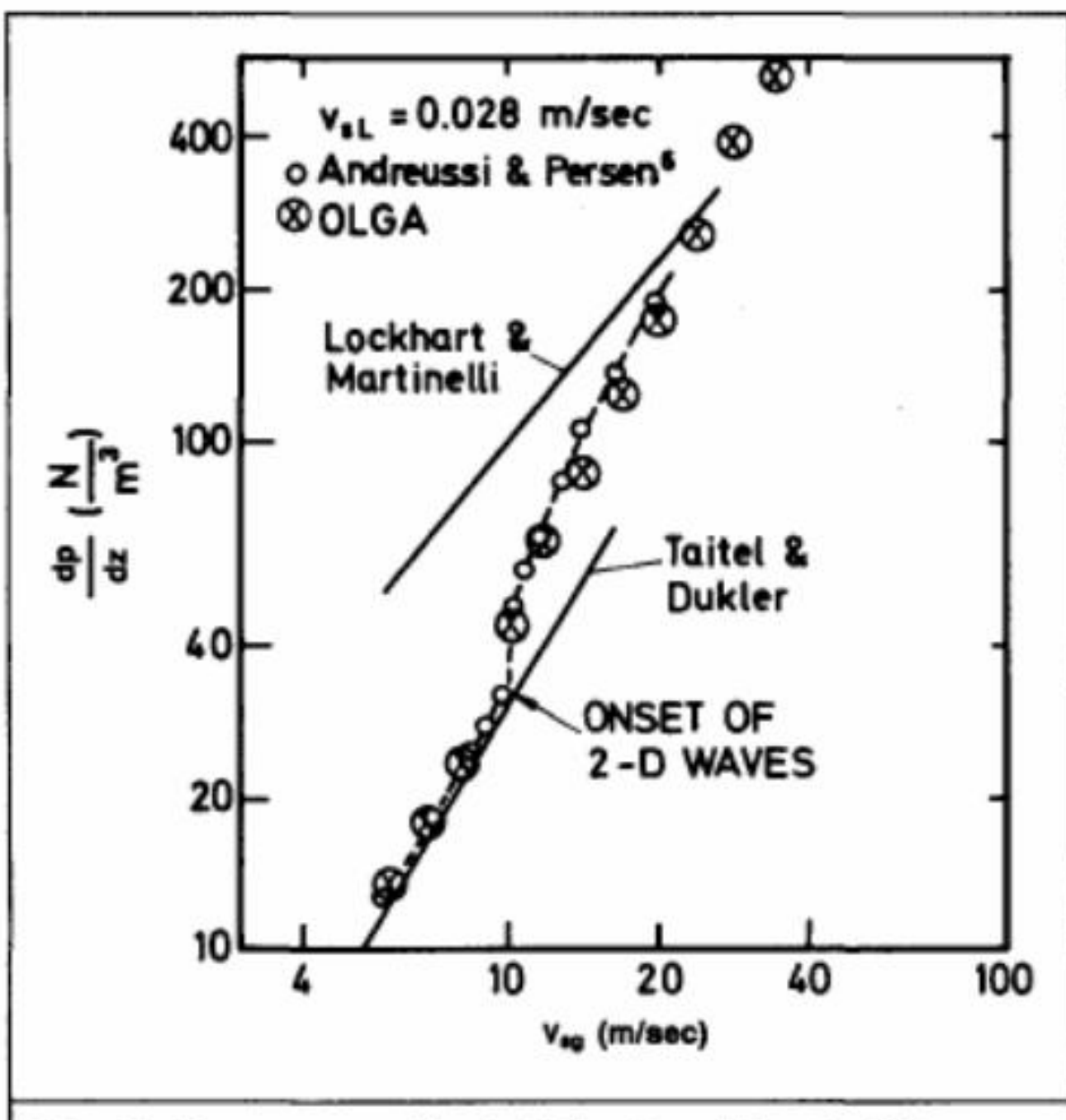


Fig. 3—Pressure gradient at the transition to 2D waves [ $\mu_L = 0.001 \text{ kg}/(\text{sec}\cdot\text{m})$ ,  $\alpha = -0.65^\circ$ ].

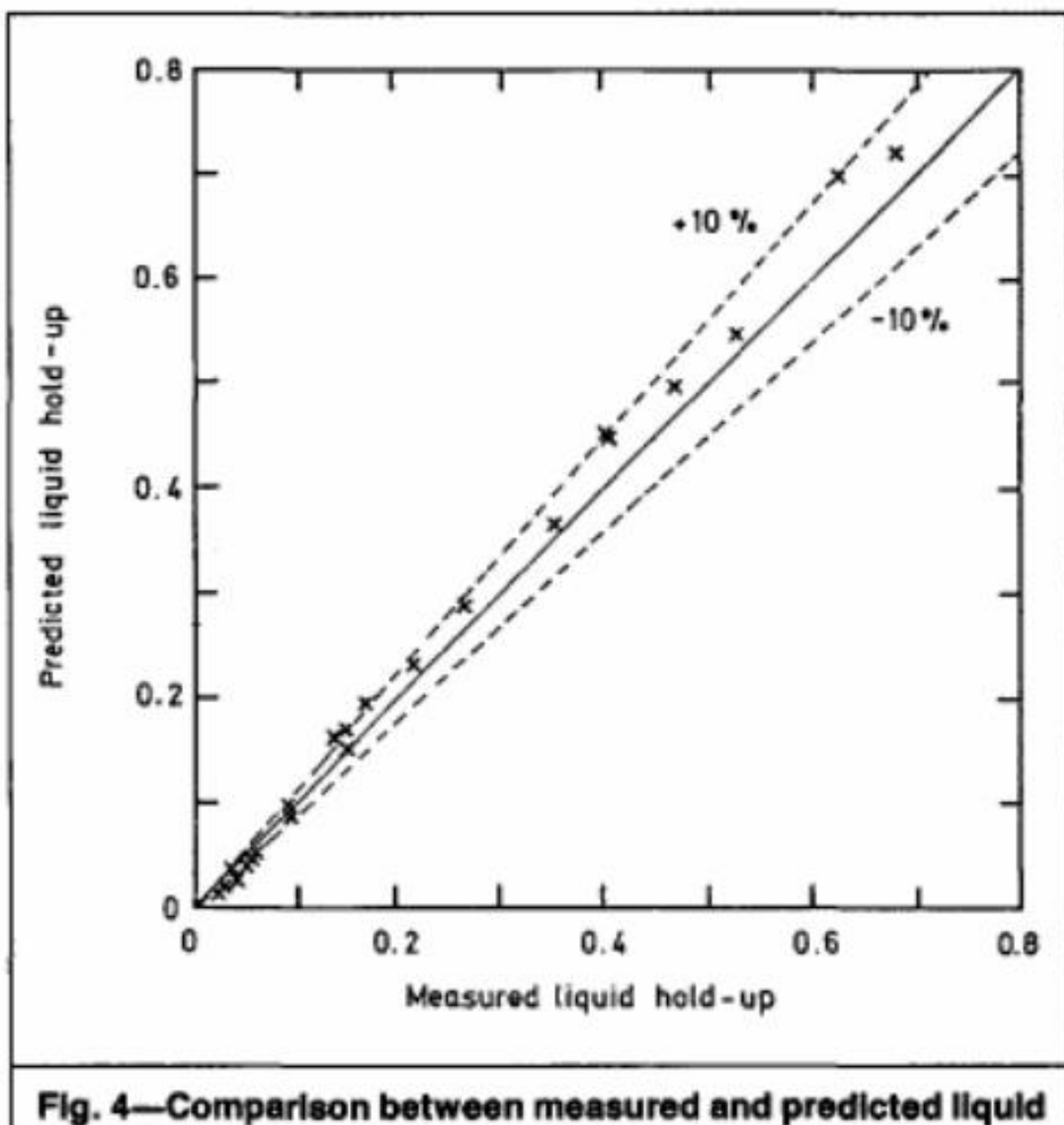


Fig. 4—Comparison between measured and predicted liquid holdup [diesel and nitrogen horizontal stratified flow at  $3 \times 10^6 \text{ Pa}$  and  $30^\circ\text{C}$ ; (X) OLGA].

$$\text{and } \lambda_i = 64/N_{Re}, \quad \dots \quad (24)$$

where  $\epsilon$  = absolute pipe roughness and  $d_h$  = hydraulic diameter.

For stratified-mist flow, the wall liquid fraction, wetted perimeters, and other flow parameters are defined by the wetted angle,  $\beta$ , as indicated in Fig. 2.

Wallis<sup>7</sup> proposed the following equation for interfacial friction in annular flow:

$$\lambda_i = 0.02[1 + 75(1 - V_g)], \quad \dots \quad (25)$$

which has been applied for vertical flow. For inclined pipes, Eq. 26 is used for annular-mist flow:

$$\lambda_i = 0.02(1 + KV_L), \quad \dots \quad (26)$$

where  $K$  is an empirically determined coefficient of the form

$$K = K \left\{ \frac{h_f}{d}, \left[ \frac{\sigma}{g(\rho_L - \rho_g)} \right] \right\}. \quad \dots \quad (27)$$

For stratified smooth flow, the standard friction factors with zero pipe roughness are used; for wavy flow, the minimum value of Eq. 26 and

$$\lambda_i = h_w/d_{hi} \quad \dots \quad (28)$$

are used because Eq. 26 is assumed to yield an upper limit for wavy flow. Eq. 28 then provides an improved description in the region from smooth flow to higher velocities, where Eq. 26 applies.

**Entrainment/Deposition.** A droplet field was not incorporated into the original version of OLGA. Compared with the SINTEF Two-Phase Flow Laboratory data, the predicted pressure drops in vertical annular flow were up to 50% too high (Fig. 1). In horizontal flow, the pressure drop was well predicted, but the liquid holdup was too high by a factor of two in extreme cases.

For droplet deposition, the following equation for vertical flow may be obtained from Andreussi's<sup>8</sup> data:

$$\psi_d = \frac{4}{d} \frac{V_D \rho_L}{V_g} 2.3 \times 10^{-4} \left( \frac{\rho_L}{\rho_g} \right)^{0.8} \left( 1 + \frac{1}{0.1 + v_{sl}} \right). \quad \dots \quad (29)$$

For inclined pipes another, extended correlation is applied.

A modified expression is proposed for liquid entrainment based on that of Dallman *et al.*<sup>9</sup> for vertical flow and Laurinat *et al.*<sup>10</sup> for horizontal flow.

**Distributed Flow.** As Malnes<sup>11</sup> showed, in the general bubble- or slug-flow case, the average phase velocities satisfy the following slip relation:

$$v_g = R_D(v_L + v_r), \quad \dots \quad (30)$$

where  $v_r$  and  $R_D$  are determined from continuity requirements. For  $V_{gS}=0$ , Eq. 30 reduces to the general expression for pure slug flow:

$$v_g = \frac{1 - V_g}{(1/C_0) - V_g} \left[ v_L + \frac{v_{0b}}{C_0(1 - V_g)} \right]. \quad \dots \quad (31)$$

For fully developed turbulent slug flow with sufficiently large slug lengths ( $\geq 10D$ ), Bendiksen<sup>12</sup> showed that the velocity of slug (or Taylor) bubbles,  $v_b$ , may be approximated for all inclinations by

$$v_B = C_0(v_{sL} + v_{sg}) + v_{0b}, \quad \dots \quad (32)$$

$$\text{where } C_0 = \begin{cases} 1.05 + 0.15 \cos^2 \alpha & \text{for } N_{Fr} < 3.5 \\ 1.20 & \text{for } N_{Fr} > 3.5 \end{cases} \quad \dots \quad (33)$$

$$\text{and } v_{0b} = \begin{cases} v_{0V} \cos \alpha + v_{0H} \sin \alpha & \text{for } N_{Fr} < 3.5 \\ v_{0V} \cos \alpha & \text{for } N_{Fr} > 3.5 \end{cases}, \quad \dots \quad (34)$$

where  $v_{0V}$  and  $v_{0H}$  are the bubble velocities in stagnant liquid (neglecting surface tension) in vertical and horizontal pipes, respectively:

$$v_{0V} = 0.35\sqrt{gd} \quad \dots \quad (35)$$

$$\text{and } v_{0H} = 0.54\sqrt{gd}. \quad \dots \quad (36)$$

For pure bubble flow, Eq. 30 reduces to

$$v_g = R(v_L + v_{0S}), \quad \dots \quad (37)$$

$$\text{where } R = (1 - V_g)/(K - V_{gS}) \quad \dots \quad (38)$$

and  $K = 1/C_0$  is a distribution parameter.

Malnes<sup>13</sup> gives the average bubble-rise velocity as

$$v_{0S} = 1.18 \left[ \frac{g\sigma(\rho_L - \rho_g)}{\rho_L^2} \right]^{1/4} [(1 - V_g)|\cos \alpha|]^{1/2} \quad \dots \quad (39)$$

with positive values upward.

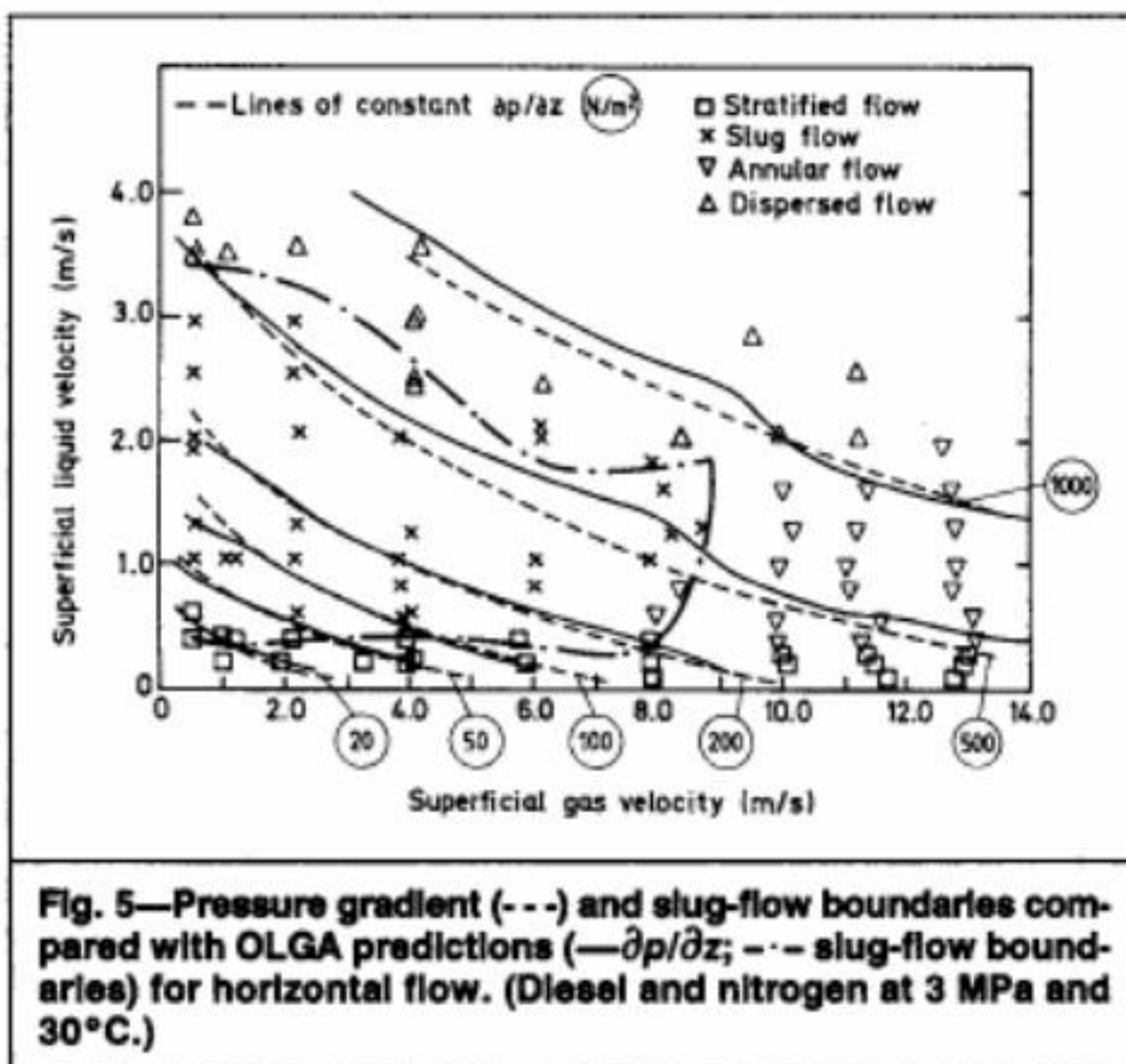


Fig. 5—Pressure gradient (---) and slug-flow boundaries compared with OLGA predictions (— $\partial p/\partial z$ ; - - - slug-flow boundaries) for horizontal flow. (Diesel and nitrogen at 3 MPa and 30°C.)

Using Gregory and Scott's<sup>14</sup> data, Malnes<sup>11</sup> proposed the following equation for the void fraction in liquid slugs:

$$V_{gS} = \frac{v_{sg} + v_{sl}}{C + v_{sg} + v_{sl}}, \quad (40)$$

where  $C$  is a constant determined empirically and the void fraction is limited upward.

This correlation (Eq. 40) is applied for small-scale systems only. For high-pressure, large-diameter pipes, another set of empirical correlations based on the data from the SINTEF Two-Phase Flow Laboratory was used.

The total pressure drop in slug flow consists of three terms:

$$(\partial z/\partial p) = (1/L)(\Delta p_s + \Delta p_b + \Delta p_{ac}), \quad (41)$$

where  $\Delta p_s$  = frictional pressure drop in the liquid slug,  $\Delta p_b$  = frictional pressure drop across the slug bubble, and  $\Delta p_{ac}$  = acceleration pressure drop required to accelerate the liquid under the slug bubble, with velocity  $v_{Lb}$  up to the liquid velocity in the slug,  $v_{LS}$  ( $\Delta p_{ac} = 0$  at present).  $L$  is the total length of the slug and bubble. These terms are dependent on the slug fraction, the slug bubble void fraction, and the film velocity under the slug bubble. The void fraction in the slug bubble,  $V_{gb}$ , is obtained by treating the flow in the film under the slug bubble as stratified or annular flow. This is further described by Malnes,<sup>11</sup> who gives additional equations. For slug flow, the wall friction terms will be more complicated than shown in Eqs. 6 and 7 because liquid friction will be dependent on  $v_g$  and the gas friction on  $v_L$ .

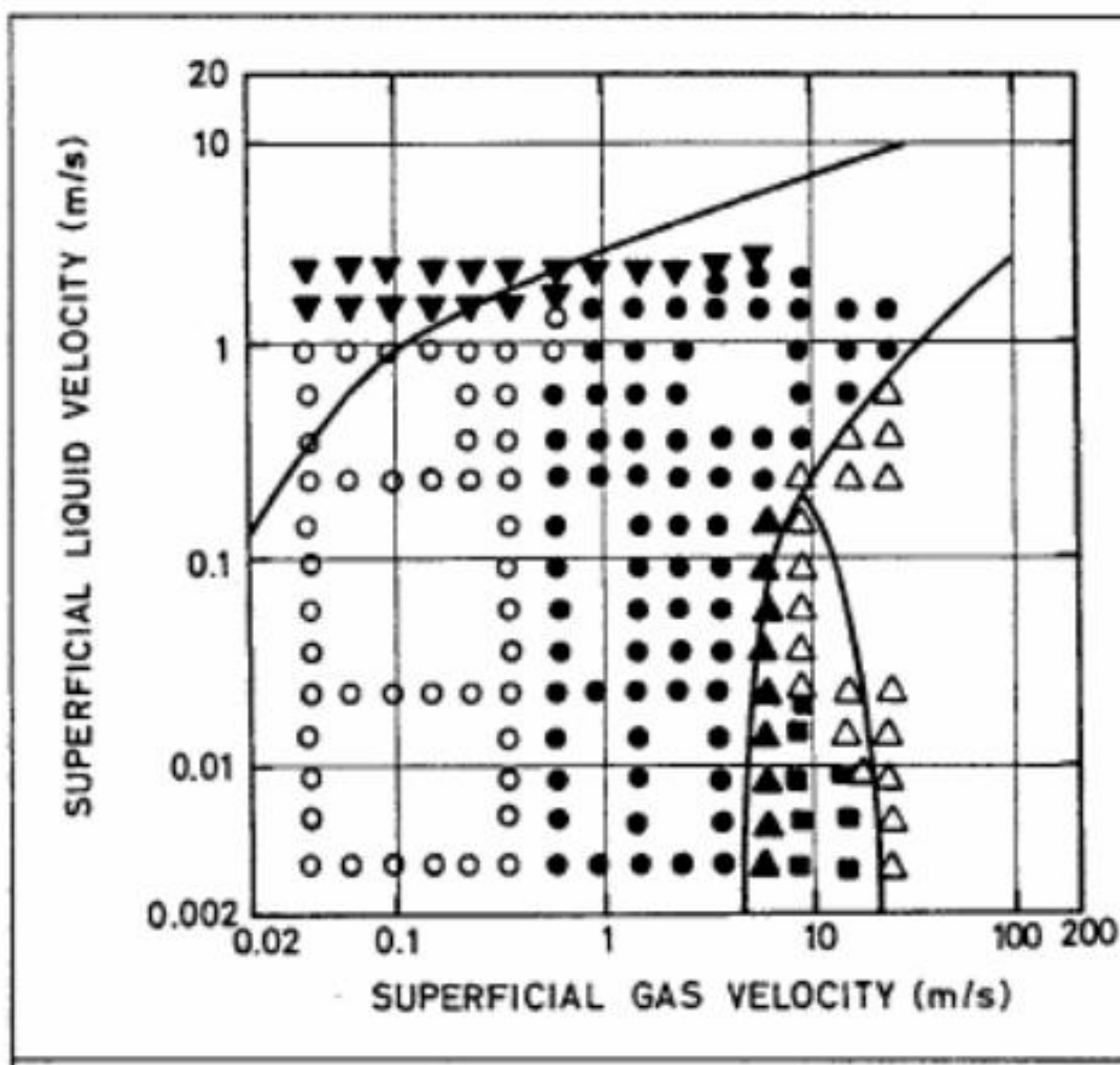


Fig. 6—Flow-regime transitions from Ref. 17 compared with OLGA [2° upward inclination, 2.5-cm ID; (—) OLGA flow-regime transition].

Flow-Regime Transitions. As stated, the friction factors and wetted perimeters are dependent on flow regime. The transition be-

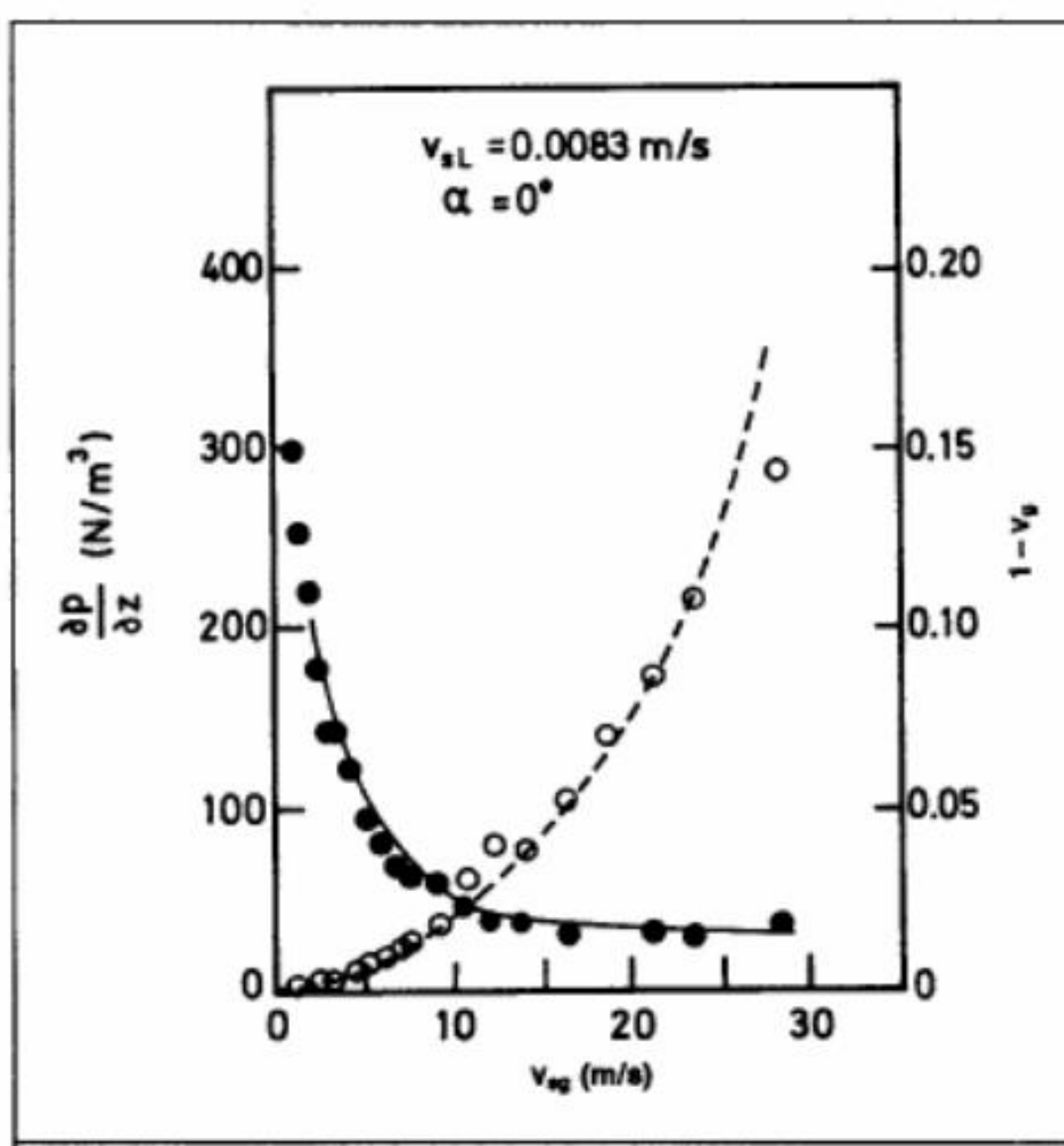


Fig. 7—Comparisons of pressure and liquid holdup—OLGA predictions (—) and Crouzier's measurements (ID = 0.045 m; ● stratified pressure drop; ▲ slug pressure drop; ○ stratified holdup; △ slug holdup).

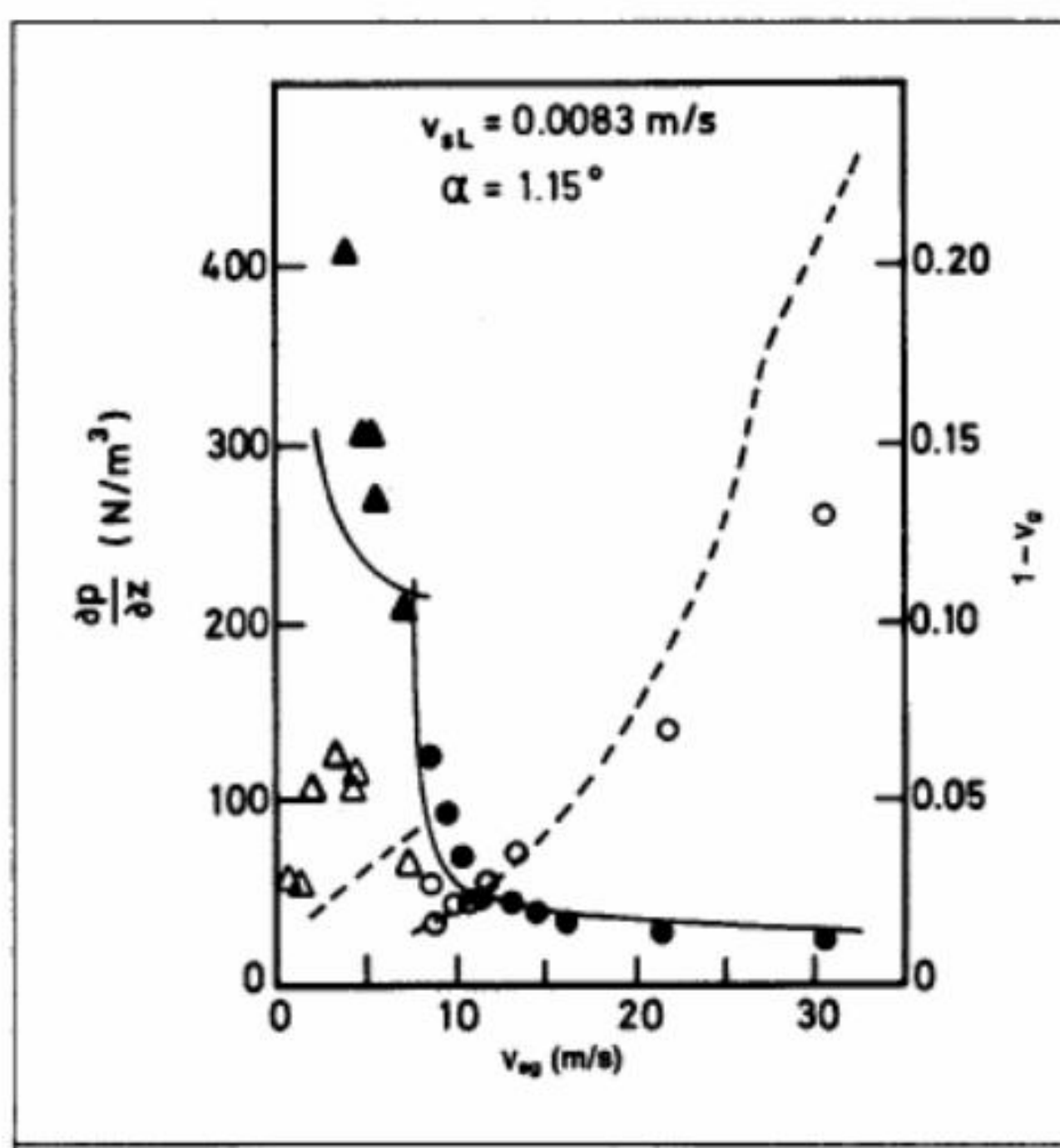


Fig. 8—Comparisons of pressure and liquid holdup—OLGA predictions (—) and Crouzier's measurements (ID = 0.045 m; ● stratified pressure drop; ▲ slug pressure drop; ○ stratified holdup; △ slug holdup).

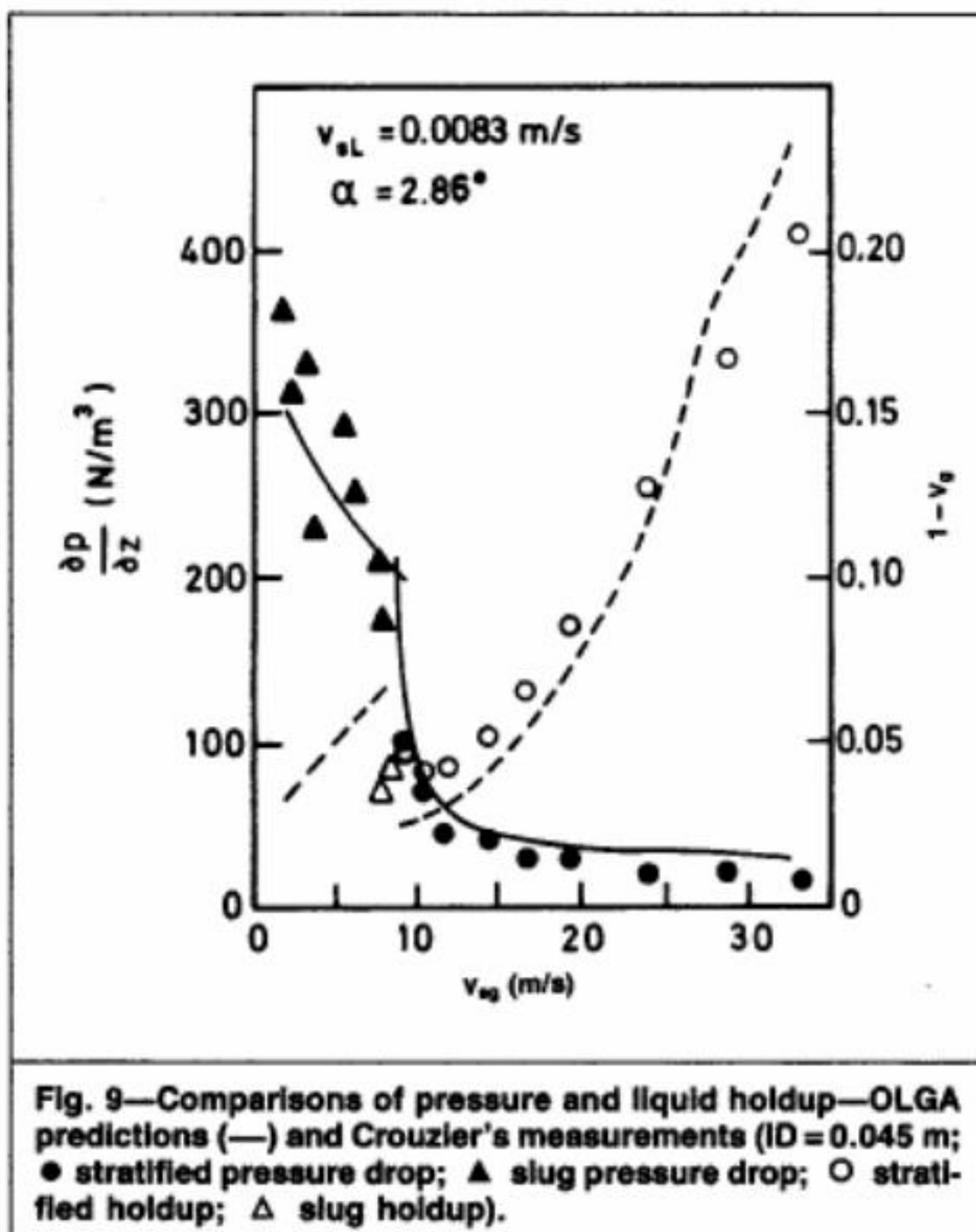


Fig. 9—Comparisons of pressure and liquid holdup—OLGA predictions (—) and Crouzier's measurements (ID = 0.045 m; ● stratified pressure drop; ▲ slug pressure drop; ○ stratified holdup; △ slug holdup).

tween the distributed and separated flow-regime classes is based on the assumption of continuous average void fraction and is determined according to a minimum-slip concept. That is, the flow regime yielding the minimum gas velocity is chosen. Wallis<sup>15</sup> empirically found a similar criterion to describe the transition from annular to slug flow very well. This criterion covers the transitions from stratified to bubble flow, stratified to slug flow, annular to slug flow, and annular to bubble flow.

In distributed flow, bubble flow is obtained continuously when all the gas is carried by the liquid slugs (when the slug fraction,  $F_S$ , approaches unity). This occurs when the void fraction in the liquid slug,  $V_{gS}$ , becomes larger than the average void fraction,  $V_g$ .

The stratified-to-annular flow transition is obtained when the wave height,  $h_w$  (Eq. 22) reaches the top of the tube (or  $S_L = \pi D$ ).

#### Comparison With Steady-State Experiments

OLGA has been compared with data from different experimental facilities, covering a wide range of geometrical sizes, fluid types, pressure levels, and pipe inclinations. The bulk of the data was obtained from experiments at the SINTEF Two-Phase Flow Laboratory. These unique data have increased our confidence in the applied two-phase models. A detailed description of the experimental facilities is presented in Bendiksen *et al.*<sup>16</sup>

Fig. 4 (from Ref. 16) compares predicted and measured holdup for stratified flow for diesel and nitrogen at  $3 \times 10^6$  Pa and 30°C. The predictions are generally within  $\pm 10\%$ .

Fig. 5 compares OLGA-predicted pressure gradients and slug-flow boundaries with data from the SINTEF Two-Phase Flow Laboratory. The predictions are quite good, although the pressure drop in the aerated slugs is somewhat low.

Barnea *et al.*<sup>17</sup> measured flow patterns for air/water flow in horizontal and inclined tubes at near-atmospheric conditions for 1.95- and 2.55-cm diameters. Fig. 6 shows a typical example of predicted flow regime transitions compared with the experimental flow map for +2° inclination.

Crouzier<sup>18</sup> measured pressure drop and holdup in horizontal and upwardly inclined pipes for air/water at near-atmospheric pressures in a 4.5-cm tube.

In Figs. 7 through 9, OLGA predictions are compared to Crouzier's data. The calculated and measured pressure drop and holdup generally agree quite well, considering the spread in data. The flow-regime transitions are observed when the holdup calculations for slug flow cross the predictions from stratified/annular mist. The regime with minimum holdup is that predicted by OLGA, and the agreement is quite good.

The pressure drop from slug/bubble to stratified-/annular-mist flow experiences a discontinuity at upsloping angles, which is justified partly by the experiments.

#### Comparison With Dynamic Experiments

The OLGA model has been compared with data from two different types of experimental setups. Schmidt *et al.*<sup>19</sup> performed experiments at laboratory conditions with a pipeline ID of 5.08 cm at atmospheric pressure. The SINTEF Two-Phase Flow Laboratory has been producing data for gas and oil in 19-cm-ID pipes with total lengths of 450 m at pressures up to 10 MPa (Fig. 10).

**Terrain-Slugging Data.** Terrain slugging is a transient flow type associated with low flow rates. It may, for instance, be observed in pipelines where a downsloping pipe terminates in a riser. The slugging is initiated by liquid accumulating at the low point. Refs. 19 and 20 give more detailed descriptions of the phenomenon.

**SINTEF Two-Phase Flow Laboratory Data.** The test section of the SINTEF laboratory is sketched in Fig. 10; further details are given in Refs. 16 and 21. In the reported experiments, the fluids applied were diesel oil and nitrogen.

One terrain-slugging flow map obtained with OLGA is shown in Fig. 11 for a system pressure of 3 MPa. The agreement with the experimental map is quite good, although the OLGA predictions are somewhat conservative for low liquid superficial velocities. Note that OLGA can properly distinguish between the two types of terrain slugging (I, II) with or without aerated slugs.

**Data of Schmidt *et al.*** This nitrogen/kerosene low-pressure loop included a nearly horizontal pipe and a vertical riser test section of 30- and 15-m lengths, respectively, and 5-cm diameters. Schmidt *et al.*'s<sup>19</sup> test matrix was reproduced for downsloping pipes, particularly for -5°, inclination. The results are shown in Fig. 12, where the solid lines are the results of the OLGA simulations. Fig.

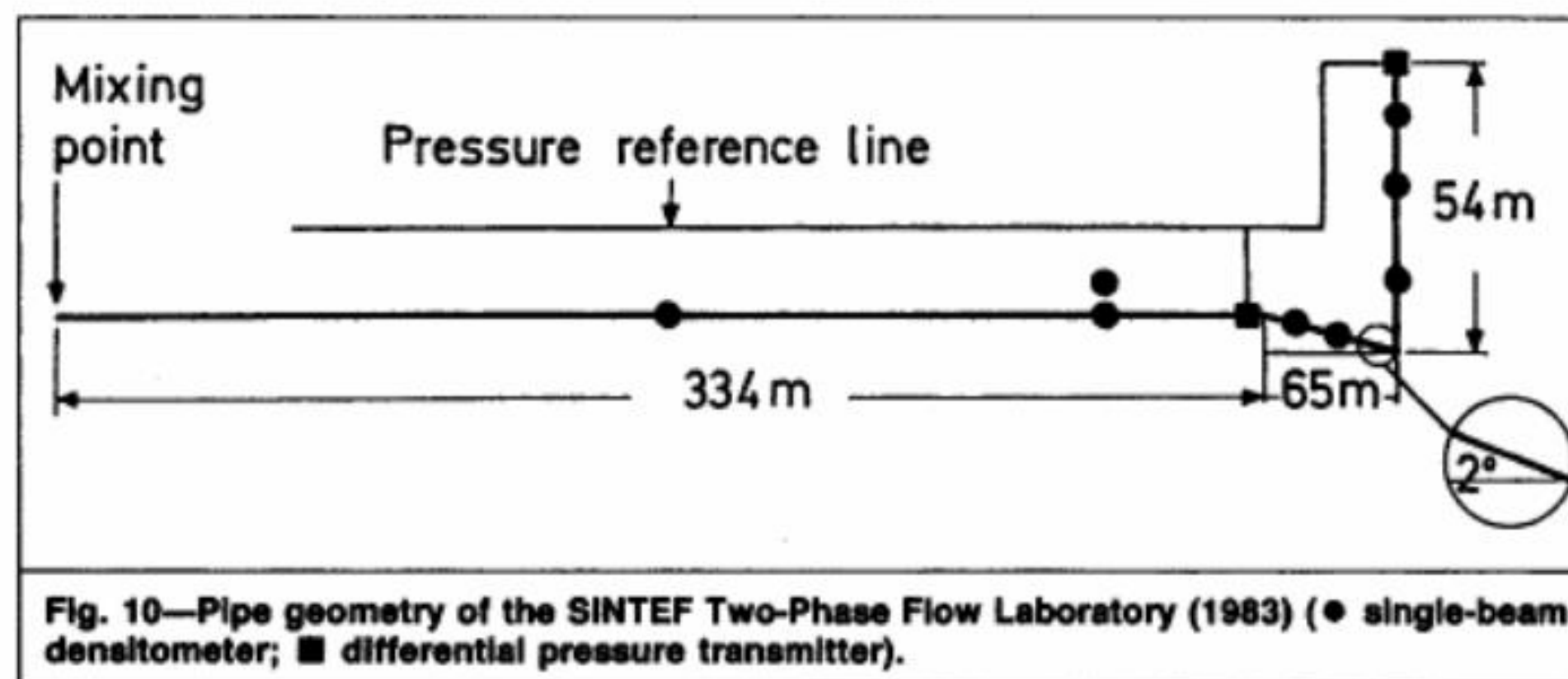


Fig. 10—Pipe geometry of the SINTEF Two-Phase Flow Laboratory (1983) (● single-beam densitometer; ■ differential pressure transmitter).

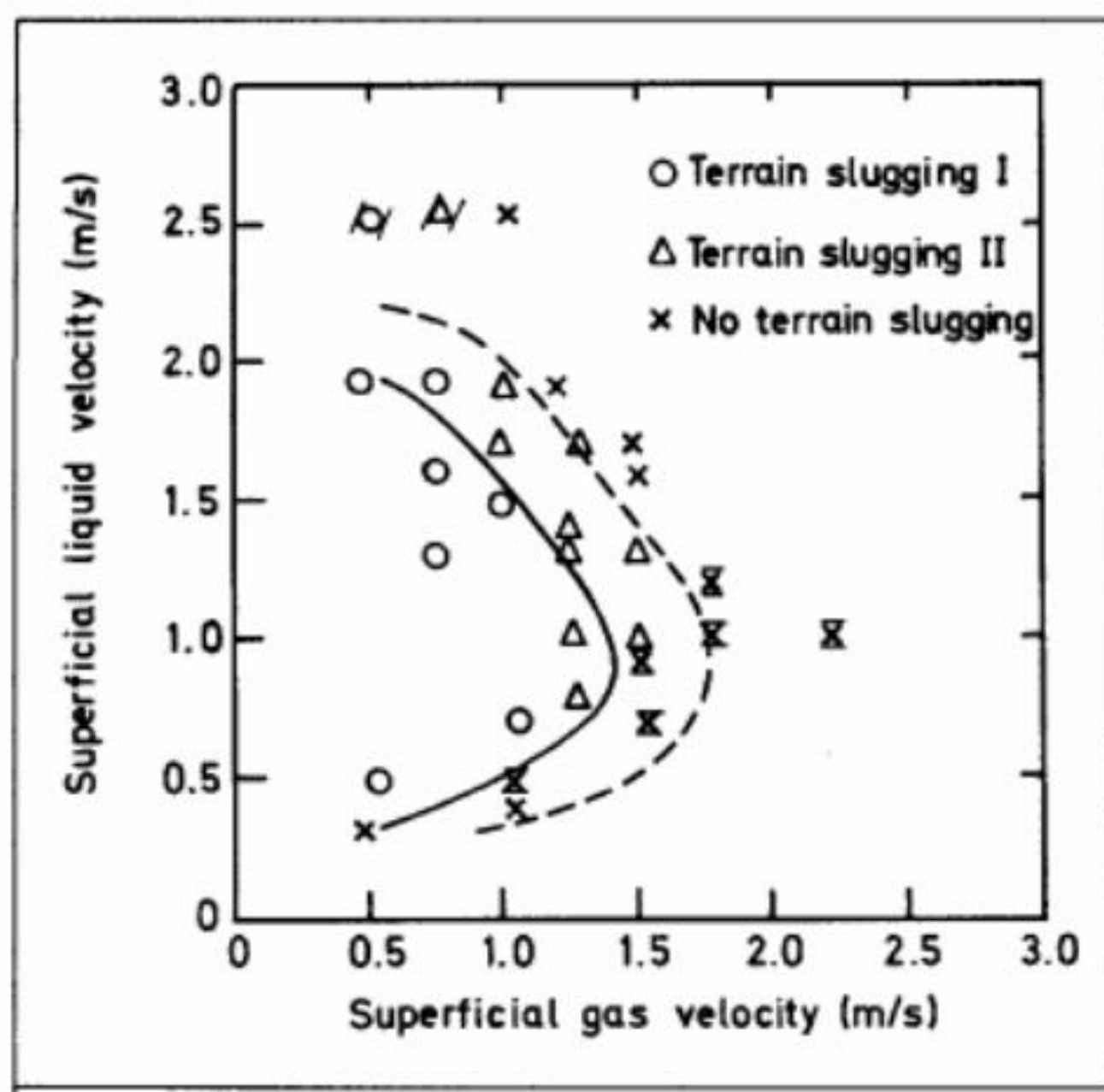


Fig. 11—Terrain-sludging flow map from the SINTEF Two-Phase Flow Laboratory. Terrain sludging I (—) and II (---) boundaries predicted by OLGA.

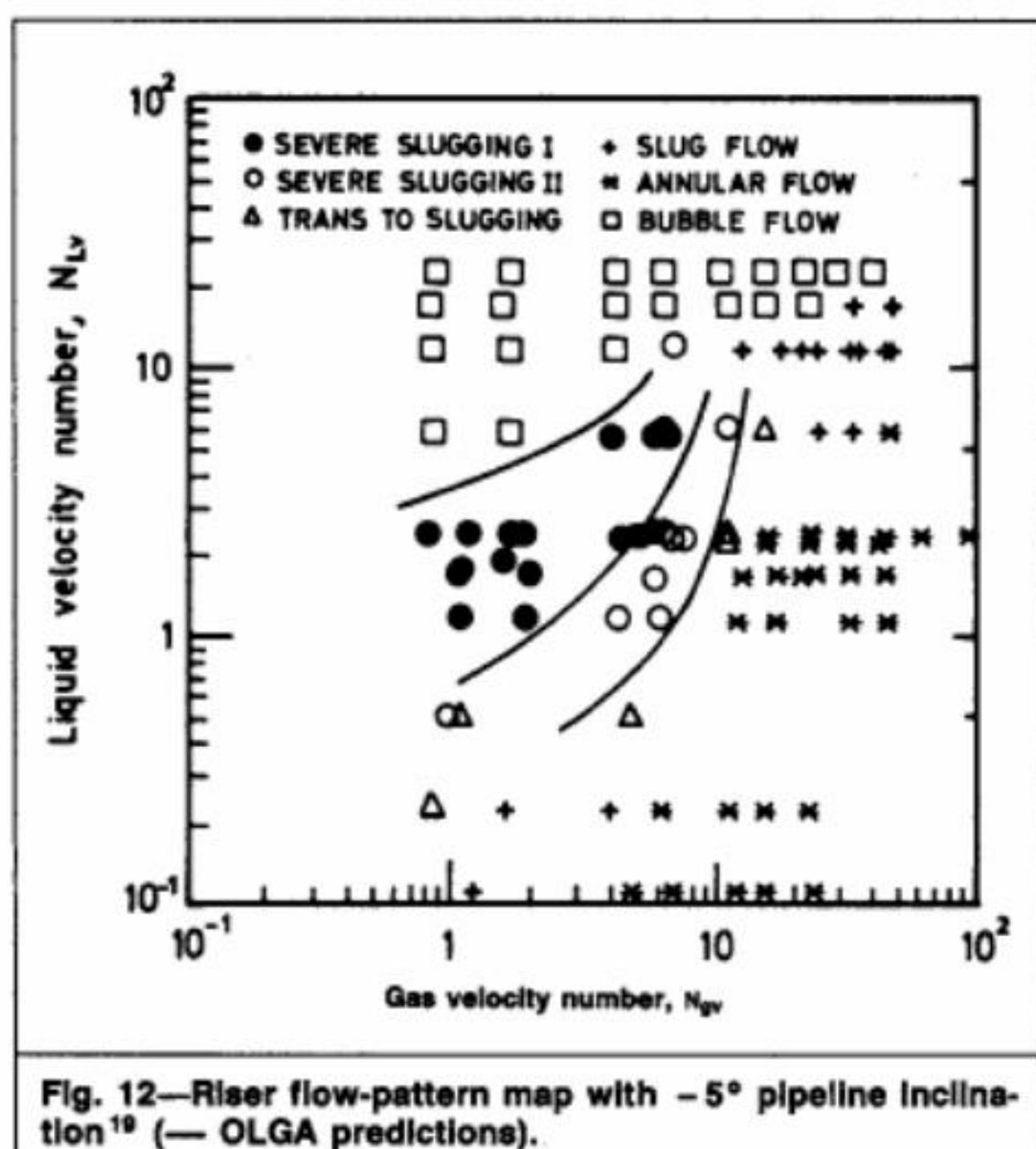


Fig. 12—Riser flow-pattern map with -5° pipeline inclination<sup>19</sup> (— OLGA predictions).

13 compares experimental and predicted pressure oscillations in the horizontal line and at the bottom of the riser for one particular experiment.

**Transient Inlet-Flow Data.** The dynamic experiments in the SINTEF laboratory with time-dependent inlet flow rates were performed with a completely horizontal flowline terminating into the riser<sup>22</sup> (see Fig. 14). The fluids were naphtha and nitrogen. The inlet liquid superficial velocity was kept constant at 1.08 m/s, while the superficial gas velocity was increased from 1.0 to about 4.2 m/s in a period of 20 seconds (Fig. 15).

The increase in the gas flow rate results in a decrease in the liquid holdup. This discontinuity in liquid holdup tends to be smeared out and broken up into slugs as it travels along the pipeline. The OLGA model applies a mean-slug-flow description but clearly is

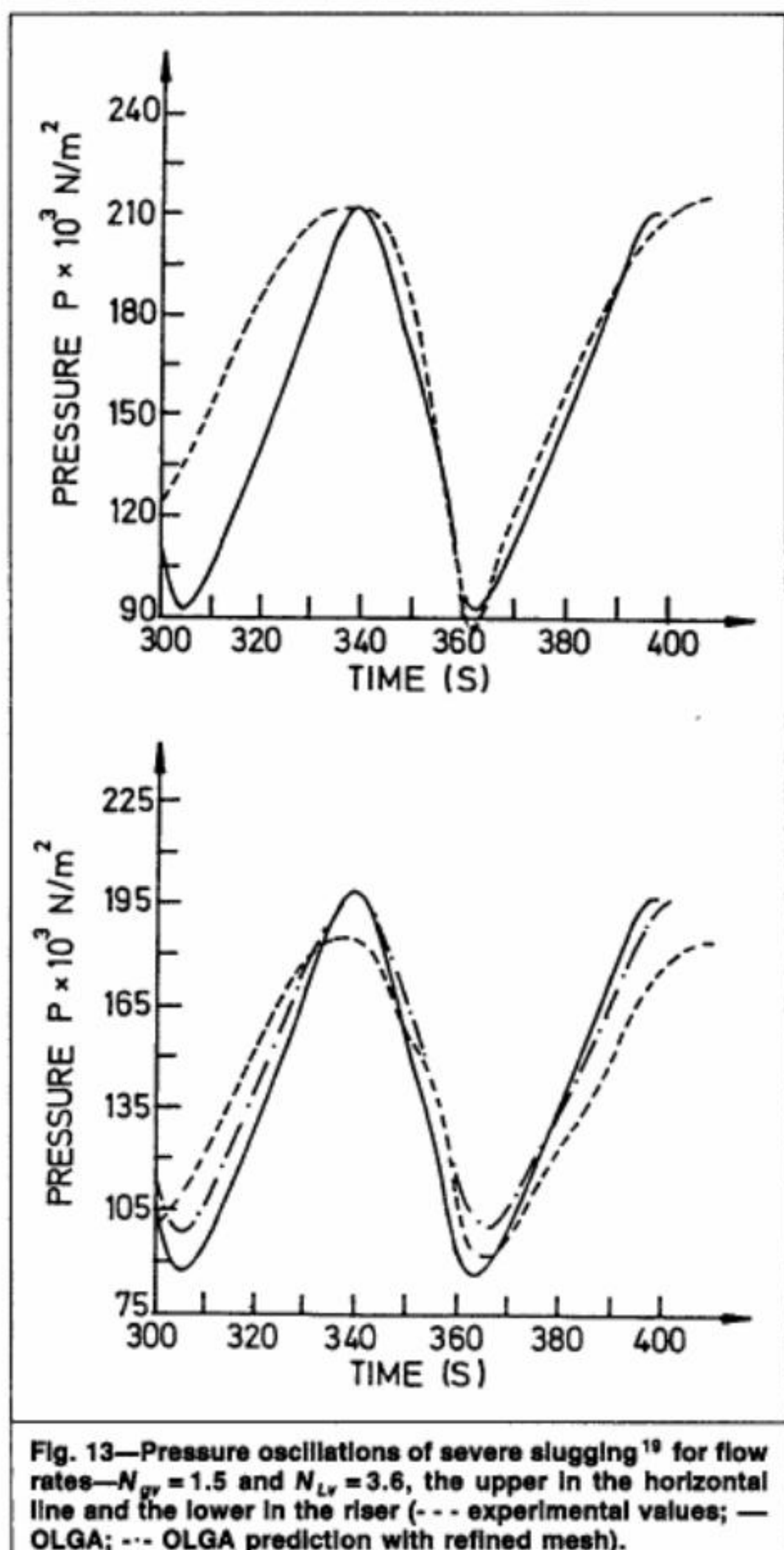


Fig. 13—Pressure oscillations of severe slugging<sup>19</sup> for flow rates— $N_{Gv} = 1.5$  and  $N_{Lv} = 3.6$ , the upper in the horizontal line and the lower in the riser (— experimental values; — OLGA; --- OLGA prediction with refined mesh).

able to simulate the time evolution of holdup and the pressure response to the inlet conditions (Figs. 16 through 20). The predicted time response is good, but slightly too slow.

#### Excerpts of Comparisons Against Field Data

To test the extrapolation capabilities of OLGA, a separate study was performed, comparing this model with evaluated field data.<sup>4</sup> The results of one of these studies, the Vic Bilh-Lacq oil/associated-gas line, are presented here. This is an onshore field of relatively heavy crude in southwestern France.

The pipeline is 43.8 km long and has a 25.1-cm ID, and an absolute roughness of 0.03 mm. Flow conditions are characterized by low superficial liquid velocities of about 0.17 m/s and superficial gas velocities ranging from 0.02 to 0.4 m/s. See Refs. 23 and 24 for further details. The inclines are very steep, resulting in upsloping sections almost filled with oil and downsloping ones nearly filled with gas. Because of the very low velocities, the pressure drop is dominated by gravity in the upsloping parts, with a slight recovery in the downsloping parts.

Pressure-drop data are reported along the pipeline at four locations for a pressure at Lacq of 1.7 MPa and a flow rate of 700 m<sup>3</sup>/d, which has been assumed to represent a total mass flow of 7.28 kg/s. In Table 1, the results from OLGA (Version 87.0) and

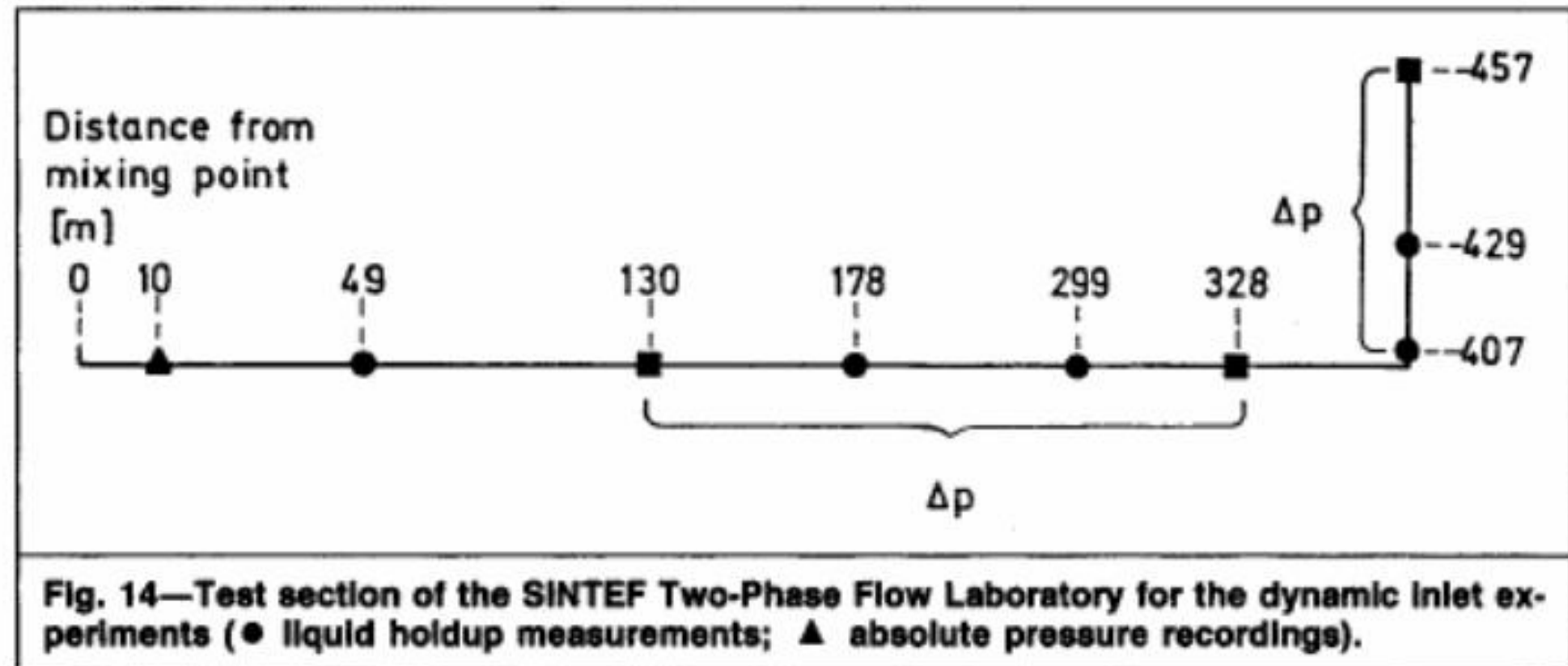


Fig. 14—Test section of the SINTEF Two-Phase Flow Laboratory for the dynamic inlet experiments (● liquid holdup measurements; ▲ absolute pressure recordings).

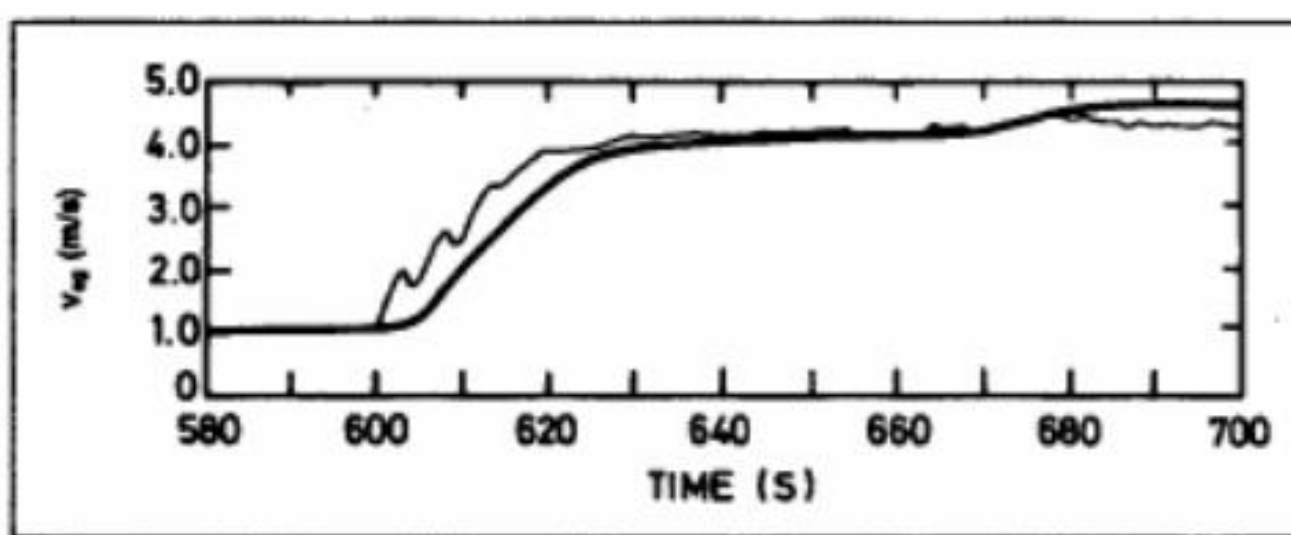


Fig. 15—Superficial-gas-velocity recordings for the dynamic inlet-flow experiments at the SINTEF Two-Phase Flow Laboratory (— applied in OLGA).

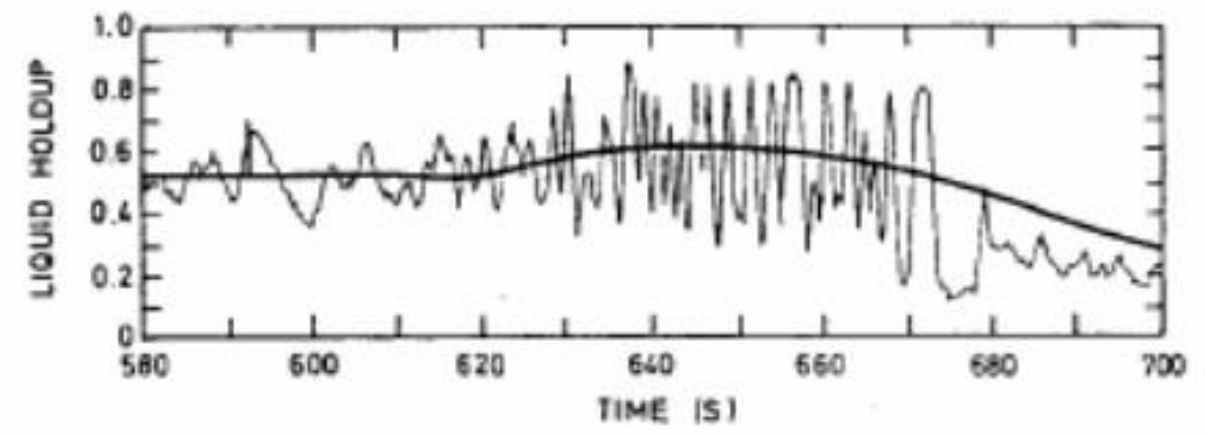
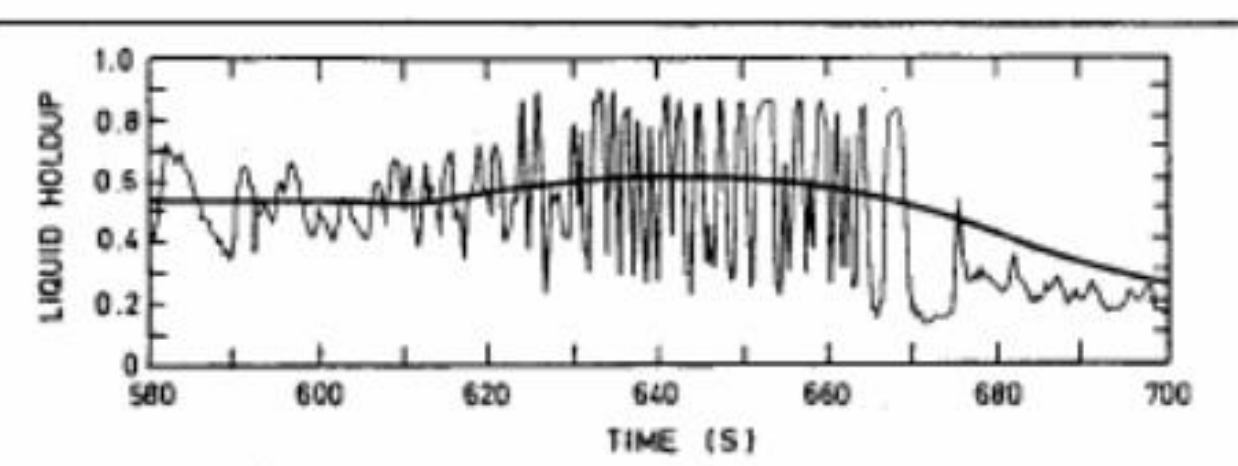


Fig. 17—Liquid-holdup recordings in the riser compared with OLGA (—) at locations 7 and 29 m from the riser bottom.

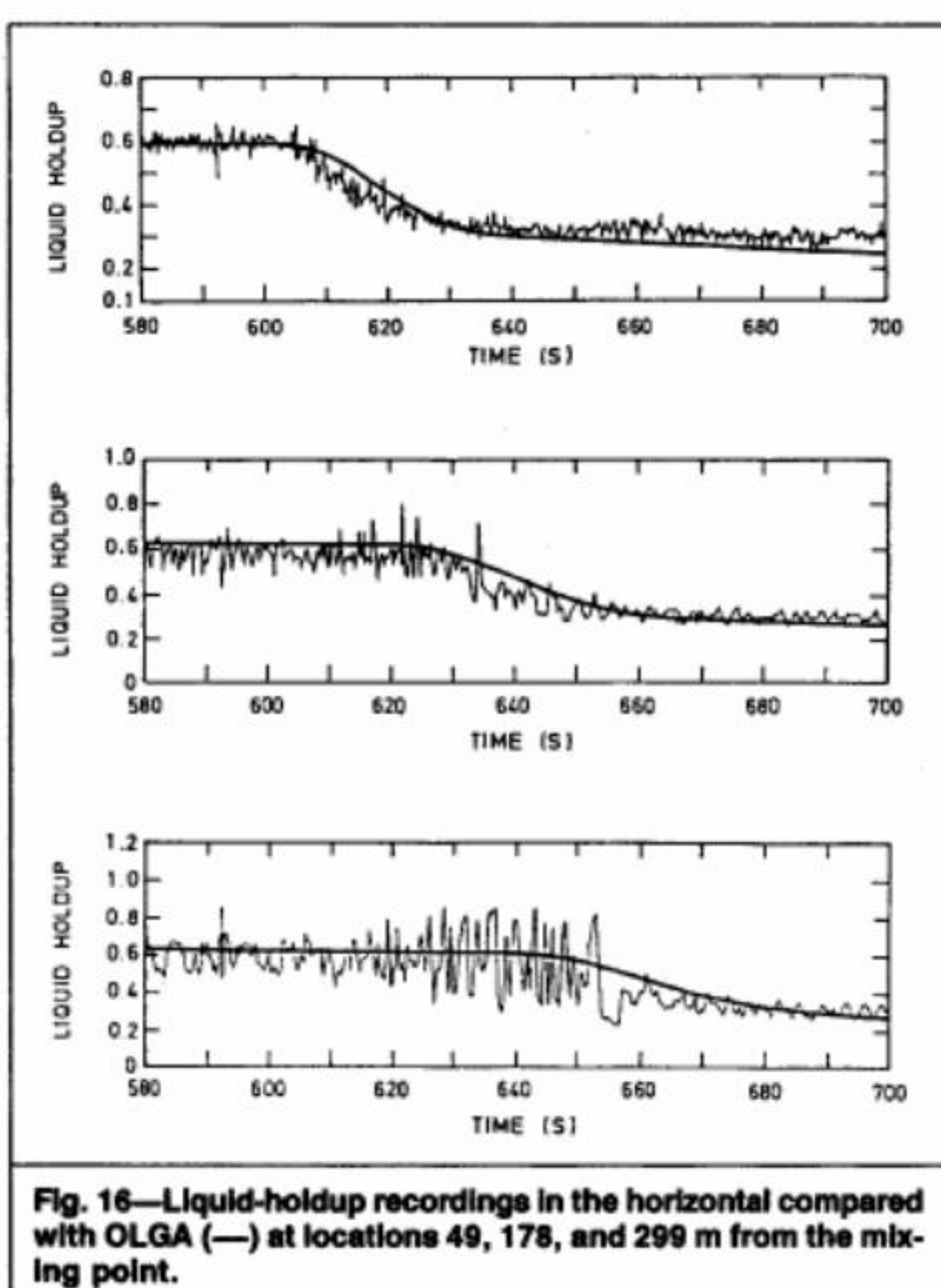


Fig. 16—Liquid-holdup recordings in the horizontal compared with OLGA (—) at locations 49, 178, and 299 m from the mixing point.

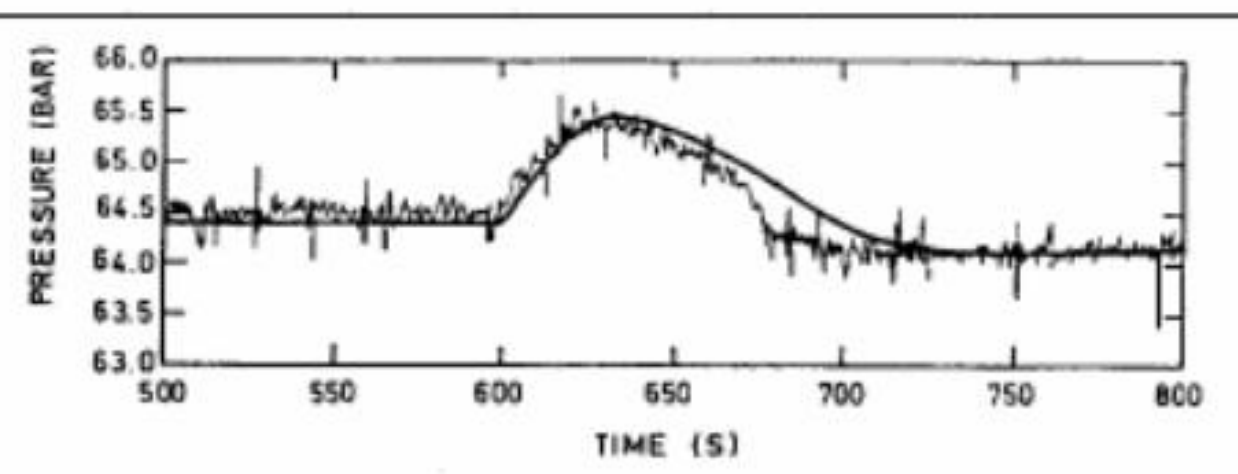


Fig. 18—Absolute pressure recorded 10 m from the mixing point compared with OLGA (—).

sure drop from PEPITE is even lower than the OLGA values, or 28% too low.

The discrepancies were found to result from the terrain profile reported by Lagière *et al.* being too coarse. Table 2 shows new, substantially improved results from OLGA based on a more detailed pipeline profile obtained from TOTAL.

### Conclusions

The OLGA model was presented, with emphasis on the particular two-fluid model applied and the flow-regime description. The importance of including a separate droplet field was discussed. Neglecting the droplet field in vertical annular flow was shown to overpredict pressure by 50% in typical cases.

Closure laws are still, at best, semimechanistic and require experimental verification.

The OLGA model has been tested against experimental data over a substantial range in geometrical scale (diameters from 2.5 to 20 cm, some at 76 cm; pipeline length/diameter ratios up to 5,000;

the steady-state model PEPITE<sup>23</sup> are compared with the measured values using the terrain profile reported by Lagière *et al.*<sup>23</sup>

The pressure drop calculated by OLGA is 15% too low, whereas the reported PEPITE calculations are extremely good. To check the input data, an available PEPITE version was run with the same input data used in OLGA. As can be seen from Table 1, the pres-

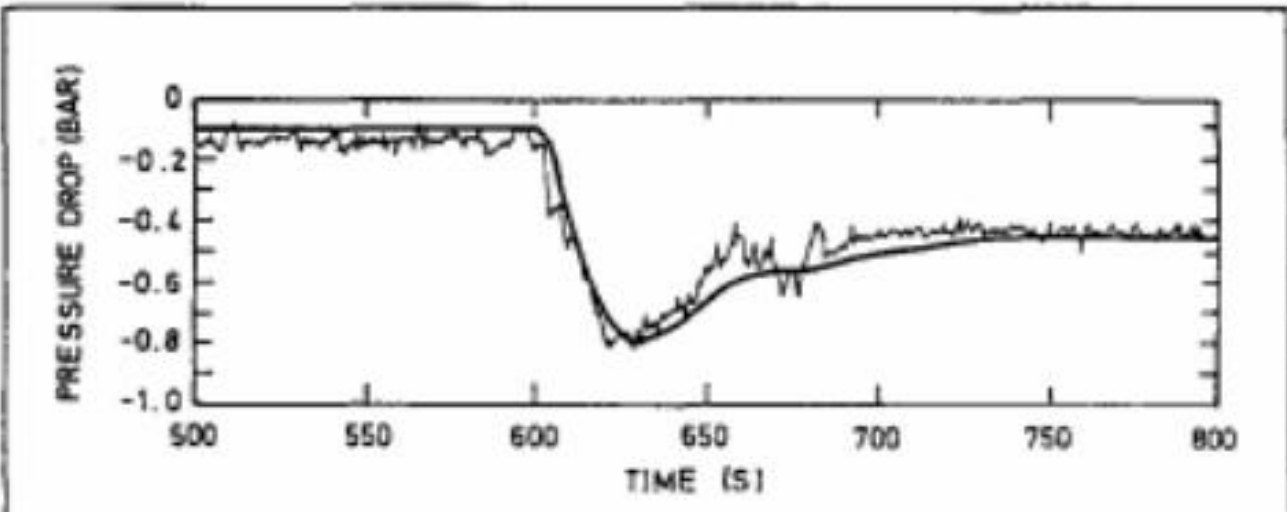


Fig. 19—Pressure difference over a part of the horizontal line compared with OLGA (—).

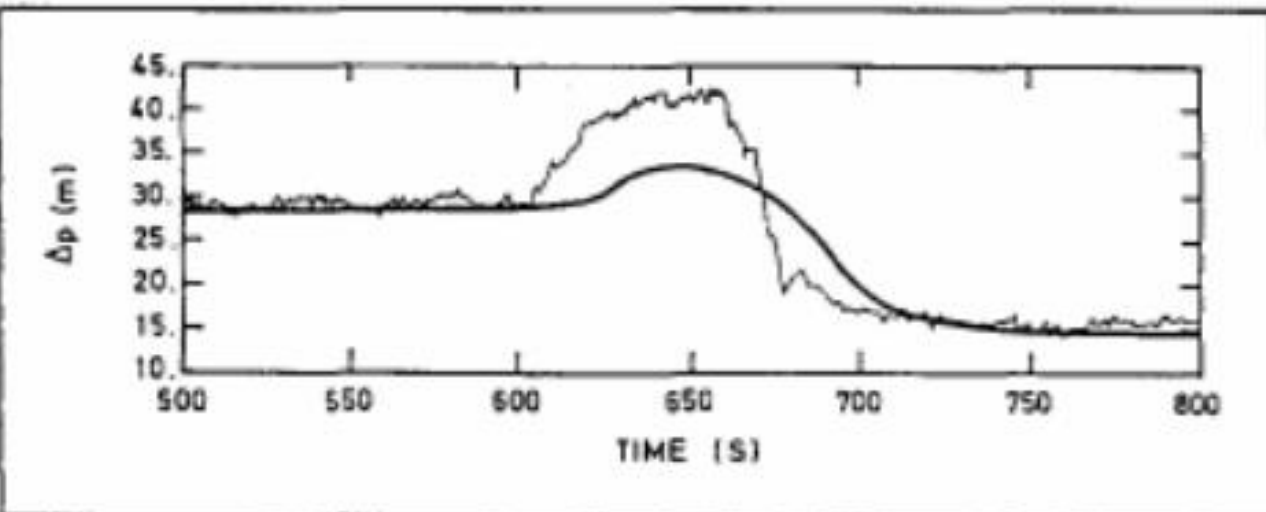


Fig. 20—The pressure difference over the riser compared with OGIA (—) (the pressure difference is recalculated as equivalent liquid height).

and pipe inclinations of  $-15$  to  $+90^\circ$ , pressures from 100 kPa to 10 MPa, and a variety of different fluids.

The model gives reasonable results compared with transient data in most cases. The predicted flow maps and the frequencies of terrain slugging compare very favorably with experiments.

The model was also tested on a number of different oil and gas field lines. The OLGA predictions are generally in good agreement with the measurements. The Vic Bilh-Lacq oil/associated-gas line was a good test case because of the extremely hilly terrain and low flow rates, which imply that, to obtain a correct pressure drop, the liquid holdup prediction must be very accurate. The pressure drop predicted by OLGA was 6.85 MPa compared with a measured drop of 6.8 MPa.

The actual number of available field lines where the fluid composition and line profile are sufficiently well documented for a meaningful comparison is, however, still limited. Further verification of this type of two-phase flow models is clearly needed.

### Nomenclature

- $A$  = pipe cross-sectional area,  $\text{m}^2$
- $c$  = speed of sound,  $\text{m}/\text{s}$
- $C$  = constant
- $C_0$  = distribution slip parameter
- $d$  = diameter,  $\text{m}$
- $E$  = internal energy per unit mass,  $\text{J}/\text{kg}$
- $F_D$  = drag force,  $\text{N}/\text{m}^3$
- $F_S$  = slug fraction,  $L_S/(L_B+L_S)$
- $g$  = gravitational constant,  $\text{m}/\text{s}^2$
- $G$  = mass source,  $\text{kg}/\text{s} \cdot \text{m}^3$
- $h$  = height,  $\text{m}$
- $h_f$  = average film thickness,  $\text{m}$
- $H$  = enthalpy,  $\text{J}/\text{kg}$
- $H_S$  = enthalpy from mass sources,  $\text{J}/\text{kg}$
- $K$  = coefficient, distribution slip parameter
- $L$  = length,  $\text{m}$
- $m_D$  =  $V_D \rho_L$ ,  $\text{kg}/\text{m}^3$
- $m_g$  =  $V_g \rho_g$ ,  $\text{kg}/\text{m}^3$
- $m_L$  =  $V_L \rho_L$ ,  $\text{kg}/\text{m}^3$
- $N$  = number
- $N_{Fr}$  = Froude number
- $N_{Re}$  = Reynolds number
- $p$  = pressure,  $\text{N}/\text{m}^2$
- $\Delta p$  = pressure drop,  $\text{N}/\text{m}^2$

- $R$  = slip ratio
- $R_D$  = distribution slip ratio
- $R_S$  = gas/oil mass ratio
- $S$  = perimeter,  $\text{m}$
- $S_f$  = wetted perimeter, Phase  $f$ ,  $\text{m}$
- $t$  = time, seconds
- $\Delta t$  = timestep, seconds
- $T$  = temperature,  $^\circ\text{C}$
- $U$  = heat transfer per unit volume,  $\text{J}/\text{m}^3$
- $v$  = velocity,  $\text{m}/\text{s}$
- $v_b$  = velocity of large slug bubble,  $\text{m}/\text{s}$
- $V_F$  = volumetric fractions ( $F=g, L, D$ )
- $z$  = length coordinate,  $\text{m}$
- $\Delta z$  = mesh size,  $\text{m}$
- $\alpha$  = angle with gravity vector, rad
- $\beta$  = angle, rad
- $\epsilon$  = absolute roughness,  $\text{m}$
- $\lambda$  = friction coefficient
- $\mu$  = viscosity,  $\text{kg}/\text{m} \cdot \text{s}$
- $\rho$  = density,  $\text{kg}/\text{m}^3$
- $\sigma$  = surface tension,  $\text{N}/\text{m}$
- $\psi$  = mass-transfer term,  $\text{kg}/\text{m}^3 \cdot \text{s}$

### Subscripts

- $ac$  = acceleration
- $b$  = bubble
- $d$  = droplet deposition
- $D$  = droplet
- $e$  = droplet entrainment
- $f$  = Phase  $f(G, L, D)$
- $F$  = friction
- $g$  = gas
- $h$  = hydraulic
- $H$  = horizontal
- $hi$  = hydraulic, interfacial
- $i$  = interfacial
- $l$  = laminar
- $L$  = liquid
- $r$  = relative
- $s$  = superficial
- $S$  = slug
- $t$  = turbulent
- $V$  = vertical
- $w$  = wave

TABLE 1—COMPARISON OF MEASURED AND PREDICTED PRESSURE DROPS ON THE VIC BILH-LACQ PIPELINE\*

Section	Length (km)	Measurement (bar)	PEPITE		OLGA (bar)
			Reported (bar)	Actual (bar)	
Vic Bilh-Claracq	8.7	18	16.9	15.5	17.7
Claracq-Morlanne	21.1	31	30.9	22.0	24.4
Morlanne-Lacq	14.0	19	18.4	12.7	15.9
Vic Bilh-Lacq	43.8	68	66.2	50.2	58.0

\*Terrain profile from Lagière et al.<sup>23</sup>

## Authors



Malnes



Bendiksen



Moe



Nuland

**K.H. Bendiksen** is head of the Dept. for Fluid Flow and Gas Technology at IFE at Kjeller, Norway. He holds an MS degree in physics and a PhD degree in fluid mechanics from the U. of Oslo, where he is also a professor of applied fluid mechanics. His technical interests include research, development, and promotion of multiphase transportation technology in the offshore oil and gas industry. He has been in charge of the OLGA development project

since its start in 1980. **Dag Malnes**, a senior research scientist at IFE, has been working with two-phase flow, heat transfer, and dynamic simulation for 30 years. He holds MS and Dr. Ing. degrees in mechanical engineering from the Norwegian Inst. of Technology. **Randi Moe** is a senior physicist at IFE, working on physical and numerical modeling of multiphase flow. She holds an MS degree in fluid flow from the U. of Oslo. **Sven Nuland** is chief engineer at IFE, where he is working on multiphase flow problems, both experiments and modeling. He has been working on the OLGA project since 1980. He holds an MS degree from the U. of Oslo.

W = wall

0 = relative zero liquid flow at infinity

## References

1. TRAC-PFI An Advanced Best Estimate Computer Program for Pressurized Water Reactor Analysis, NUREG/CR-3567, LA-994-MS (Feb. 1984).
2. RELAP5/MOD1 Code Manual Volume 1: System Models and Numerical Methods, NUREG/CR-1826, EGG-2070 (March 1982).
3. Micaelli, J.C.: 1987 CATHARE an Advanced Best-Estimate Code for PWR Safety Analysis, SETh/LEML-EM/87-58.
4. Bendiksen, K., Espedal, M., and Malnes, D.: "Physical and Numerical Simulation of Dynamic Two-Phase Flow in Pipelines with Application to Existing Oil-Gas Field Lines," paper presented at the 1988 Conference on Multiphase Flow in Industrial Plants, Bologna, Sept. 27-29.
5. Malnes, D., Rasmussen, J., and Rasmussen, L.: A Short Description of the Blowdown Program, NORA SD-129, IFE, Kjeller (1972).
6. Andreussi, P. and Persen, L.N.: "Stratified Gas-Liquid Flow in Downwardly Inclined Pipes," *Int'l. J. Multiphase Flow* (1987) 13, 565-75.
7. Wallis, G.B.: "Annular Two-Phase Flow, Part 1: A Simple Theory," *J. Basic Eng.* (1970) 59.
8. Andreussi, P.: "Droplet Transfer in Two-Phase Annular Flow," *Int'l. J. Multiphase Flow* (1983) 9, No. 6, 697-713.
9. Dallman, J.C., Barclay, G.J., and Hanratty, T.J.: "Interpretation of Entrainments in Annular Gas-Liquid Flows," *Two-Phase Momentum, Heat and Mass Transfer*, F. Durst, G.V. Tsiklauri, and N.H. Afgan (eds.).

TABLE 2—COMPARISON OF MEASURED AND PREDICTED PRESSURE DROPS ON THE VIC BILH-LACQ PIPELINE WITH NEW PROFILE

Section	Length (km)	Measurement (bar)	OLGA (bar)
Vic Bilh-Claracq	8.7	18	18.6
Claracq-Morlanne	21.1	31	32.4
Morlanne-Lacq	14.0	19	17.5
Vic Bilh-Lacq	43.8	68	68.5

10. Laurinat, J.E., Hanratty, T.J., and Dallman, J.C.: "Pressure Drops and Film Height Measurements for Annular Gas-Liquid Flow," *Int'l. J. Multiphase Flow* (1984) 10, No. 3, 341-56.
11. Malnes, D.: *Slug Flow in Vertical, Horizontal and Inclined Pipes*, IFE/KR/E-83/002 (1983).
12. Bendiksen, K.H.: "An Experimental Investigation of the Motion of Long Bubbles in Inclined Tubes," *Int'l. J. Multiphase Flow* (1984) 10, No. 4, 467-83.
13. Malnes, D.: "Slip Relations and Momentum Equations in Two-Phase Flow," IFE Report EST-1, Kjeller (1979).
14. Gregory, G.A. and Scott, D.S.: "Correlation of Liquid Slug Velocity and Frequency in Horizontal Co-Current Gas-Liquid Slug Flow," *AIChE J.* (1969) 15, No. 6, 933.
15. Wallis, G.B.: *One-Dimensional Two-Phase Flow*, McGraw Hill Book Co. Inc., New York City (1969).
16. Bendiksen, K. et al.: "Two-Phase Flow Research at SINTEF and IFE. Some Experimental Results and a Demonstration of the Dynamic Two-Phase Flow Simulator OLGA," paper presented at the 1986 Offshore Northern Seas Conference, Stavanger.
17. Barnea, D. et al.: "Flow Pattern Transition for Gas-Liquid Flow in Horizontal and Inclined Pipes," *Int'l. J. Multiphase Flow* (1980) 6, 217-26.
18. Crouzier, O.: "Ecoulements diphasiques gaz-liquides dans les conduites faiblement inclinées par rapport à l'horizontale," MS thesis, l'Université Pierre et Marie Curie, Paris (1978).
19. Schmidt, Z., Brill, J.P., and Beggs, H.D.: "Experimental Study of Severe Slugging in Two-Phase-Flow Pipeline-Riser System," *SPEJ* (Oct. 1980) 407-14.
20. Bendiksen, K., Malnes, D., and Nuland, S.: "Severe Slugging in Two-Phase Flow Systems," paper presented at the third Lecture Series on Two-Phase Flow, Trondheim, IFE Report KR/E-6, Kjeller (1982).
21. Norris, L. et al.: "Developments in the Simulation and Design of Multiphase Pipeline Systems," paper SPE 14283 presented at the 1985 SPE Annual Technical Conference and Exhibition, Las Vegas, Sept. 22-25.
22. Linga, H. and Østvang, D.: "Tabulated Data From Transient Experiments With Naphtha," SINTEF/IFE project, Report No. 41 (Feb. 1985).
23. Lagière, M., Miniscloux, C., and Roux, A.: "Computer Two-Phase Flow Model Predicts Pipeline Pressure and Temperature Profiles," *Oil and Gas J.* (April 1984) 82-92.
24. Corteville, J., Lagière, M., and Roux, A.: "Designing and Operating Two-Phase Oil and Gas Pipelines," *Proc.*, 11th World Pet. Cong., London (1983) SP 10.

## SI Metric Conversion Factors

bar	$\times 1.0^*$	E+05	= Pa
bbl	$\times 1.589\ 873$	E-01	= m <sup>3</sup>
ft	$\times 3.048^*$	E-01	= m
ft <sup>2</sup>	$\times 9.290\ 304^*$	E-02	= m <sup>2</sup>
ft <sup>3</sup>	$\times 2.831\ 685$	E-02	= m <sup>3</sup>
°F	$(^{\circ}F - 32)/1.8$		= °C
in.	$\times 2.54^*$	E+00	= cm
lbf	$\times 4.448\ 222$	E+00	= N
lbm	$\times 4.535\ 924$	E-01	= kg

\*Conversion factor is exact.

SPE

Original SPE manuscript received for review Jan. 4, 1989. Paper (SPE 19451) accepted for publication Dec. 11, 1990. Revised manuscript received April 30, 1990.